HYDRAULIC MODEL STUDY
SALT RIVER CHANNELIZATION PROJECT AT
SKY HARBOR INTERNATIONAL AIRPORT
PHOENIX, ARIZONA

Prepared for

ANDERSON - NICHOLS
Palo Alto, California

Prepared by

Y. H. Chen

Civil Engineering Department
Engineering Research Center
Colorado State University
Fort Collins, Colorado

October 1980

CER80-81-YHC-12

FOREWORD

This study was performed for the contract titled "Hydraulic Model Study, Salt River Channelization Project at Sky Harbor International Airport, Phoenix, Arizona," between Anderson-Nichols Company, Palo Alto, California and Colorado State University. This report describes in detail the physical model utilized to assess the adequacy of the Salt River Channelization Project at Sky Harbor International Airport.

The study was supervised by Dennis R. Horn, Vice President and by Benjamin R. Roberts, Study Manager, Anderson-Nichols Company, and was sponsored by the U.S. Army Corps of Engineers, Sacramento District and Federal Emergency Management Agency (FEMA), Region IX, San Francisco, California. Dr. Yung Hai Chen, Civil Engineering Department, Colorado State University, was the Principal Investigator. Dr. Daryl B. Simons, Professor of Civil Engineering Department, was the technical advisor. They were assisted by Mr. Sedat Ariman, Dr. Abbas A. Fiuzat, Mr. Mohamed R. AbdelBary, Keith D. Engell, Jacinto Rivero and Hugo Zevallos. Dr. Ruh-Ming Li, Principal Hydraulics Engineer, Simons, Li and Associates, Inc. (SLA) also provided useful information. Mrs. Margaret Reuss typed the report. The study period was from August to November, 1980.

TABLE OF CONTENTS

Chapter		Page
I.	INTRODUCTION	1
II.	MODELING THEORIES	1
	II.1. Model Scaling Ratios	3
	II.2. Bed Roughness in the Fixed-Bed Model	5
	II.3. Bed Material on the Movable-Bed Model	7
	II.4. Time Scaling Ratios for the Movable-Bed Model	8
	II.5. Determination of Levee Slope for the Movable-Boundary Model	12
III.	RIVER MECHANICS FLUME AND STUDY AREA	14
	III.1. Description of River Mechanics Flume	14
	III.2. Modeling of Study Area	18
	III.3. Instrumentation	21
IV.	RESULTS OF FIXED-BED MODEL TESTS	23
	IV.1. Stage of Physical Model Tests and Their Comparison with Mathematical Model Stages	24
	IV.2. Velocity Distributions in the Fixed-Bed Physical Model	31
	IV.3. Preliminary Evaluation of Channelization System	36
V.	MOVABLE BED MODEL TESTS	40
	V.1. Construction of the Movable-Bed Model	40
	V.2. Operation of the Movable-Bed Model	45
	V.3. Bed-Elevation Changes	48
	V.4. Stability of Levees	69
	V.5. Effects of Riverbed Changes on Hydraulics	69
VI.	CONCLUDING REMARKS	75

LIST OF TABLES

Table		Page
1	Critical Velocity, Shear Stress and Bed-Material Size	8
2	Prototype and Model Coordinate Relations	20
3	Model Test Conditions	21
4	Water Surface Elevations in the Fixed-Bed Physical Model, Q = 92,000 cfs	25
5	Water Surface Elevations in the Fixed-Bed Physical Model, Q = 176,000 cfs	26
6	Water Surface Elevations in the Fixed-Bed Physical Model, Q = 210,000 cfs	27
7	Freeboard for Q = 210,000 cfs	38
8	Step Discharges, Duration and Stages in the Movable-Bed Model	46
9	Changes in Stages between the Movable-Bed Model and the Rigid-Bed Model (Q = 210,000 cfs)	75

LIST OF FIGURES

Figure		Page
1	Size Distribution of Bed Material in the Movable-Bed Model	9
2	General Layout of the River Mechanics Flume Testing System, Branch Hydraulics Laboratory	15
3	Detailed Plan View of the River Mechanics Flume	17
4	Model and Prototype Length Coordinates	19
5	Photographs Showing the Fixed-Bed Model	22
6	Comparison between Average Stages of Fixed-Bed Physical Models and Mathematical Model Stages at Q=92,000 cfs.	28
7	Comparison between Average Stages of Fixed-Bed Physical Models and Mathematical Model Stages at Q=176,000 cfs	29
8	Comparison between Average Stages of Fixed-Bed Physical Models and Mathematical Model Stages at Q= 210,000 cfs.	30
9	Velocity Distributions in the Fixed-Bed Model at 92,000 cfs	32
10	Velocity Distributions in the Fixed-Bed Model at 176,000 cfs	33
11	Velocity Distributions in the Fixed-Bed Model at 210,000 cfs	34
12	Flow Division around the ILS	35
13	Preliminary Review of the HNTB Levee Protection Plan and Possible Modifications	39
14	Modified Cross-Sectional Shapes in the Movable-Bed Model	41
15	Photo of the Movable-Bed Model	42
16	Various Views of the Movable-Bed Model	43
17	The Initial Bed Elevations in the Movable-Bed Model	44
18	Standardized Discharge Hydrograph	47
19	Photos showing the Bed Surface of the Movable-Bed Model after Routing the First 92,000 cfs Hydrograph	49

Figure		Page
20	Photos Showing the Bed Surface of the Movable-Bed Model after Routing the Second 92,000 cfs Hydrograph . .	50
21	Bed Contours in the Movable-Bed Model after Routing the First 92,000 cfs Hydrograph	51
22	Bed Contours in the Movable-Bed Model after Routing the Second 92,000 cfs Hydrograph	52
23	Bed Elevation Changes from the Initial Values after Routing the First 92,000 cfs Hydrograph	53
24	Bed Elevation Changes from the Initial Values after Routing the Second 92,000 cfs Hydrograph	54
25	Bed Elevation Changes at Station 21.5 after Routing the 92,000 cfs Hydrographs	55
26	Bed Elevation Changes at Station 37.6 after Routing the 92,000 cfs Hydrographs	56
27	Bed Elevation Changes at Station 42.5 after Routing the 92,000 cfs Hydrographs	57
28	Bed Elevation Changes at Station 58.4 after Routing the 92,000 cfs Hydrographs	58
29	Photos showing the Bed Surface of the Movable-Bed Model after Routing the 210,000 cfs Hydrograph	60
30	Bed Contours in the Movable-Bed Model after Routing the 210,000 cfs Hydrograph	61
31	Bed Elevation Changes from the Initial Contours after the Rising Limb of the 210,000 cfs Hydrograph	62
32	Bed Elevation Changes from the Initial Contours after Routing the 210,000 cfs Hydrograph	63
33	Bed Elevation Changes at Station 21.5 after Routing the 210,000 cfs Hydrograph	64
34	Bed Elevation Changes at Station 37.6 after Routing the 210,000 cfs Hydrograph	65
35	Bed Elevation Changes at Station 42.5 after Routing the 210,000 cfs Hydrograph	66
36	Bed Elevation Changes at Station 58.4 after Routing the 210,000 cfs Hydrograph	67

Figure		Page

37 Change in the Size Distribution of Bed Material on the Model Surface 68

38 Photos showing the Unstable Sections of the North Levees 70

39 Photos showing the Unstable Sections of the South Levees 71

40 Comparison between Velocities in the Rigid-Bed Model and in the Movable-Bed Model at Station 38.5 (Q = 92,000 cfs) 72

41 Comparison between Velocities in Rigid-Bed Model and in the Movable-Bed Model at Station 55 (Q = 92,000 cfs) 72

42 Comparison between Velocities in the Rigid-Bed Model and in the Movable-Bed Model at Station 38.5 (Q = 160,000 - 176,000 cfs) 73

43 Comparison between Velocities in the Rigid-Bed Model and in the Movable-Bed Model at Station 55.4 (Q = 210,000 cfs) 73

I. INTRODUCTION

In order to assess the adequacy of the Salt River channelization project design at Sky Harbor International Airport, Phoenix, Arizona, a hydraulic model study was conducted at the River Mechanics Flume, Engineering Research Center, Colorado State University. The scope of work for the hydraulic model study is:

1. Construct a fixed bed and movable bed physical model of the study channel reach in the 40 x 120 River Mechanics Flume.

2. Conduct studies of behavior of the channel reach under flows of 92,000, 176,000 and 210,000 cfs.

3. Using the model results, suggest recommended design improvements for the channelization project.

4. Using the physical and mathematical modeling results, assist the Anderson-Nichols' staff in estimating scour, deposition, and degree of damage to the channel during floods.

5. Prepare a final report documenting the model studies and conclusions.

In this report, the theories utilized in designing the fixed-bed model and movable-bed model are described in Chapter 2. The features of the River Mechanics Flume and the physical models are described in Chapter 3. The results of the fixed-bed model and its comparison with the mathematical model results are presented in Chapter 4. The results of the movable bed model are presented in Chapter 5. Chapter 6 provides some concluding remarks.

II. MODELING THEORIES

Two models, a fixed-bed model and a movable-bed model, were utilized in this study. The fixed-bed model is easy to control and provides a

basis to study the effects of channelization considering nonuniform velocity and flow patterns, excluding the complexity due to bed and bank movement. Specifically, the fixed-bed model was utilized to determine:

1) Velocity distribution to identify levee areas that require protections and to determine extent of protections;

2) Water surface profile to check the adequacy of levee freeboard;

3) Effects of low-flow channel on the flow distribution; and

4) Effects of any other changes in the channelization structures.

The results of fixed-bed model can be extrapolated to determine the velocity distribution and water surface profiles for other flow conditions.

The movable-bed model was utilized to determine:

1) Riverbed erosion and deposition patterns during passages of flood hydrographs;

2) Effects of bed and bank changes on velocity and water surface profiles and then on the levee stability; and

3) That one additional complexity of the 1 to 5 distorted movable-bed model is that the slope of levee has to be reduced to establish adequate levee stability. This could affect the velocity, stage as well as sediment transport patterns. The results of the movable boundary model were compared with the fixed-bed model results to evaluate the effects due to this distortion. It should be pointed out that distorted fixed-bank movable-bed models have been utilized to study the erosion and deposition problems. However, no attempts have been made to also distort the bank slope to study bank stability and bed movement at the same time. Physical modelers generally agree that this is a very tricky

problem. For studying the gravel mining and I-10 stabilization structure, we will use a rigid-bank, movable-bed model, assuming that levees would be stable. This avoids the complexity due to levee erosion and provides useful information to evaluate the movable-boundary model results.

To satisfy the similarity between the model and the prototype, the roughness of fixed-bed model should be adequately simulated. The movable-bed model also requires proper simulation of bed-material transport, levee stability and scour and deposition patterns. This was accomplished by matching the incipient conditions of bed material and levees in the model with those in the prototype under different flow conditions and by determining the time scaling ratio of bed wave movement.

II.1. Model Scaling Ratios

Past studies have shown that the effect of surface tension and viscosity can be neglected when the model is sufficiently large and is tested with warm water and a relatively high Reynolds number. Therefore, the model was constructed, tested and operated as a Froude model.

The Froude number N_F for open channel is

$$N_F = \frac{V}{\sqrt{gD}} \tag{1}$$

in which V is the mean velocity at the channel cross section, D is the hydraulic depth and g is the gravitational acceleration. The flow discharge is

$$Q = VA \tag{2}$$

in which A is the cross-sectional area and V is defined above.

Also, the hydraulic depth is defined

$$D = \frac{A}{T} \tag{3}$$

in which T is the top width.

For achieving geometric, kinematic and dynamic similarity, the Froude number should be the same for the prototype and the model, that is

$$N_{Fm} = N_{Fp} \tag{4}$$

$$\frac{V_m}{\sqrt{g_m D_m}} = \frac{V_p}{\sqrt{g_p D_p}} \tag{5}$$

Subscripts "m" and "p" refer to the model and prototype respectively.

For all practical purposes the gravitational acceleration is the same in Arizona and Colorado. That is

$$g_m = g_p \tag{6}$$

Then Eq. 5 can be reduced to

$$\frac{V_m}{V_p} = \left(\frac{D_m}{D_p}\right)^{1/2} \tag{7}$$

To adequately model the study area and to achieve the study objectives, the horizontal and vertical model-to-prototype length ratios were selected to be 1 to 175 and 1 to 35 respectively. From Eq. 7, the scaling ratios for the geometric, kinematic and dynamic variables are:

VARIABLES	SCALING RATIO
1. Horizontal length	1:175
2. Vertical length	1:35
3. Time (water wave)	$1:175/\sqrt{35}$
4. Velocity	$1:\sqrt{35}$
5. Discharge	$1:(35^{3/2})\ (175)$
6. Force	$1:(35^{2})\ (175)$

II.2. Bed Roughness in the Fixed-bed Model

The bed roughness in the model was determined based on the argument that in order to obtain kinematic and dynamic similarity between the prototype and the model, the equivalent normal-flow conditions should be achieved. Manning's equation and Strickler's equation were then utilized to determine the roughness element required in the model.

Manning's equation is given as

$$V = \frac{1.486}{n} R^{2/3} S_f^{1/2} \tag{8}$$

in which n is Manning's roughness coefficient, R is the hydraulic radius, and S_f is the energy slope. The ratio of model's to prototype's roughness coefficient is then

$$\frac{n_m}{n_p} = \left(\frac{R_m}{R_p}\right)^{2/3} \left(\frac{S_{fm}}{S_{fp}}\right)^{1/2} \left(\frac{V_p}{V_m}\right) \tag{9}$$

From Froude's Model Law

$$\frac{V_p}{V_m} = \left(\frac{D_p}{D_m}\right)^{1/2} \tag{10}$$

Also

$$\frac{R_p}{R_m} \simeq \frac{D_p}{D_m} \tag{11}$$

Substituting Eqs. 10 and 11 into Eq. 9 yields

$$\frac{n_m}{n_p} = \left(\frac{D_m}{D_p}\right)^{1/6} \left(\frac{S_{fm}}{S_{fp}}\right)^{1/2} \tag{12}$$

Based on a size analysis of composite bed-material samples provided by Dames and Moore and Howard Needles Tammen & Bergendoff (HNTB), Simons, Li and Associates (SLA) developed a size distribution of subsurface bed-material in the prototype channel having d_{16} = 2.6 mm, d_{50} = 60 mm,

d_{75} = 160 mm, d_{84} = 210 mm and d_{90} = 230 mm. This prototype size distribution was utilized to size the bed material in the fixed-bed model as well as in the movable-bed model. Meyer-Peter and Muller transformed Strickler's formula to determine Manning's roughness coefficient

$$n = \frac{d_{90}^{1/6}}{26} \tag{13}$$

where d_{90} is the diameter of sediment particles in meters for which 90 percent of the particles are finer by weight. For the prototype with d_{90} = 230 mm, n_p = 0.03. This value and the value of D_m/D_p (= 1/35) are substituted into Eq. 12 to yield

$$n_m = 0.0164 \left(\frac{S_{fm}}{S_{fp}}\right)^{1/2} \tag{14}$$

Applying Eq. 14 for different ratios of S_{fm}/S_{fp}, the following values for n_m and d_{90m} are obtained.

S_{fm}/S_{fp}	n_m	d_{90} (mm)
1	0.0164	6.0
1.8	0.0220	35.1
2	0.0232	48.1
3	0.0284	162.3
4	0.0328	384.7
5	0.0367	751.3

The horizontal and vertical length scales utilized in this model study would automatically result in a slope ratio S_{fm}/S_{fp} = 5. To obtain adequate surface roughness for this ratio, the d_{90} would be 751.3 mm,

which was not acceptable. Considering the availability of gravel materials and flume dimensions, it was decided to use 1.5-inch gravel to cover the riverbed of rigid-bed model. This requires a reduction of S_{fm}/S_{fp} from 5 to 1.8. The average bed slope of prototype is about 0.0022. Then the required model slope is 0.0040. The correction in the model slope is thus (1.8 - 5) x 0.0022 = -0.0070. This slope correction value was utilized to correct the model elevations to form the desired bed slope of 0.0040.

II.3. Bed Material in the Movable-bed Model

To adequately model the erosion and deposition patterns, the incipient motion of bed material in the model should be comparable to that in the prototype. Shield's relation for beginning of motion is

$$\frac{\tau_c}{(\gamma_s - \gamma)} = 0.047 \qquad (15)$$

in which τ_c is the critical bed shear stress defined as ($\tau = \frac{1}{8} f \rho V^2$), f is the Darcy-Weisbach resistance coefficient, ρ is the water density, $(\gamma_s - \gamma)$ is the unit weight of submerged sediment.

An "f" value of 0.08, which corresponds to the required Manning's n and a "γ_s" value of 165 lbs/ft^2 were substituted into Eq. 15 to obtain a relation between critical velocity, shear and bed-material size as shown in Table 1. To obtain adequate incipient motion of the bed material in the movable-bed model, its size distribution should have $d_{50} \simeq 2.0$ mm, $d_{75} \simeq 4.5$ mm and $d_{84} \simeq 7.0$ mm. After contacting various gravel companies in the Fort Collins area, it was found that the gravel material available locally that had the closest size distribution, was a 1/4-inch chip. The size distribution of this material was determined from a sieve analysis as shown in Fig. 1. The d_{50}, d_{75}, and d_{84} are 3.0 mm, 4.5 mm and 5.4 mm,

TABLE 1. Critical Velocity, Shear Stress and Bed-Material Size

Prototype			Model		
V_{cp} (fps)	τ_{cp} (lbs/ft^2)	d_{cp} (mm)	V_{cm} (fps)	τ_{cm} (lbs/ft^2	d_{cm} (mm)
6.5	0.82	52	1.10	0.023	1.5
8.0	1.24	78	1.35	0.035	2.2
10.4	2.10	133	1.76	0.060	3.8
12.5	3.03	192	2.11	0.086	5.4
13.5	3.54	224	2.28	0.101	6.4
15.0	4.37	276	2.54	0.125	7.9
16.0	4.96	314	2.70	0.141	8.9
20.0	7.76	490	3.38	0.222	14.0

respectively. The value of d_{50} is larger and the value of d_{84} is smaller than that desired. Therefore the simulation of armor effects at local scour areas could be somewhat off. However, it is believed that the movable-bed model should be capable of simulating the overall erosion and deposition pattern reasonably well.

Because of the reduction in bed material size utilized in the movable-bed model, its surface roughness would be smaller than that in the fixed-bed model. However, the form roughness in the movable-bed model might increase the resistance to flow to reach a reasonable agreement in effects of bed roughness.

II.4. Time Scaling Ratios for the Movable-Bed Model

The erosion and deposition patterns in the prototype channel are significantly affected by the shape of hydrograph. It is therefore

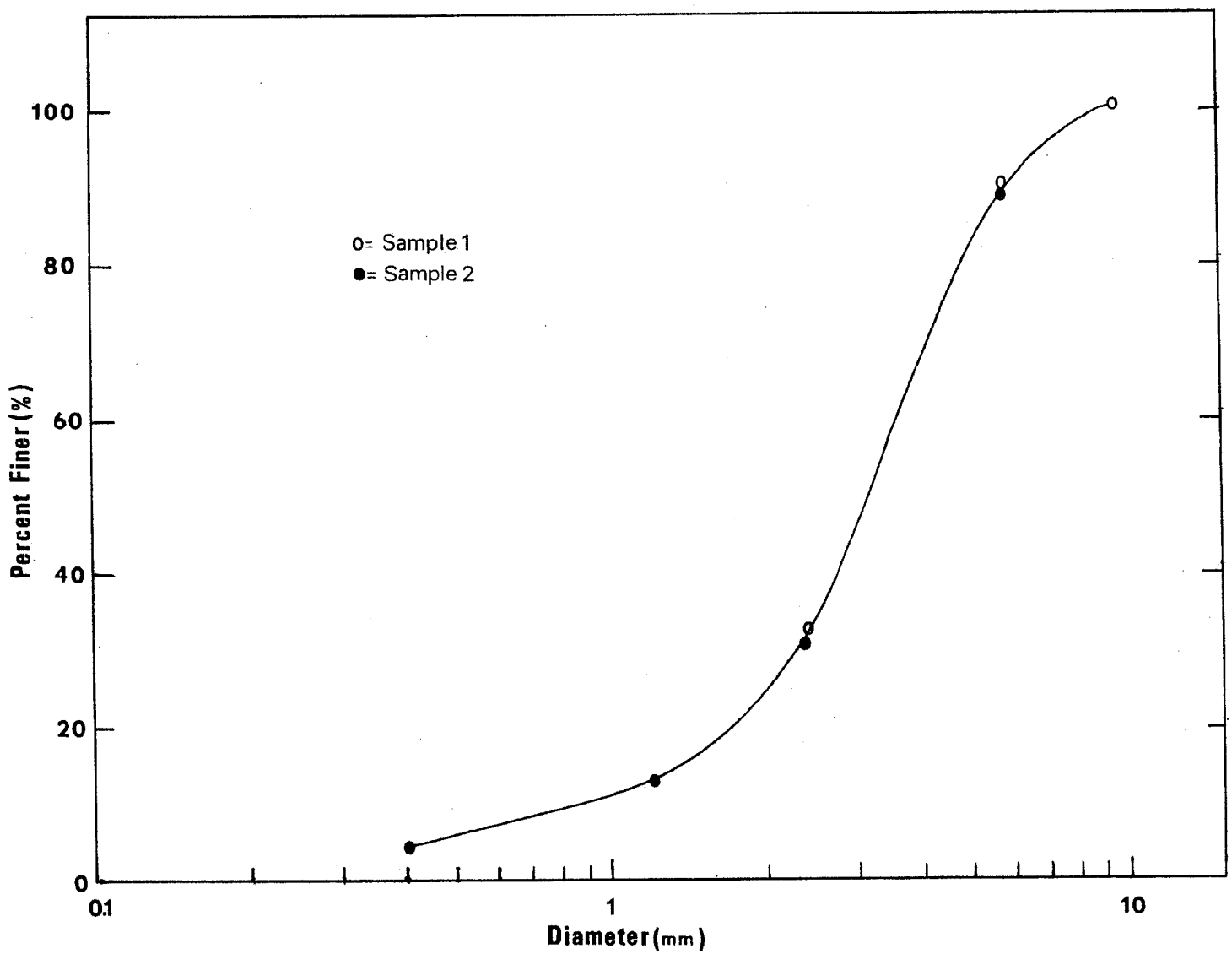

Fig. 1. Size Distribution of Bed Material in the Movable-bed Model

required to run a hydrograph through the movable-bed model. An attempt was made to convert the prototype hydrograph to a corresponding model hydrograph using a selected time scale conversion factor by comparing the celerities of bed wave in the model and prototype.

The Meyer-Peter, Muller formula was utilized to determine bed load discharge

$$q_b = \frac{8}{\sqrt{\rho}\ (\gamma_s - \gamma)} (\tau - \tau_c)^{1.5} \tag{16}$$

in which q_b is the unit-width bed load in cfs/ft, and τ is the bed shear stress in lbs/ft^2. The following power relations were obtained:

1) d = 60 mm (d_{50} in prototype)

$$q_b = 1.17 \times 10^{-6}\ V^{4.64} \tag{17}$$

2) d = 3 mm (d_{50} in model)

$$q_b = 1.72 \times 10^{-5}\ V^{4.53} \tag{18}$$

The celerity of bed wave can be derived for the sediment continuity equation as

$$c_t = \frac{1}{1-\lambda} \frac{\partial q_b}{\partial z} \tag{19}$$

in which λ is the porosity, z is the bed elevation. The bed load discharge q_b can be related to velocity by a power function.

$$q_b = a\ V^b = a\left[\frac{q}{(h-z)}\right]^b \tag{20}$$

in which q is the unit-width water discharge, and h is the stage. A unit-width channel is assumed for this derivation. Taking a derivative of q_b with respect to z yields:

$$\frac{\partial q_b}{\partial z} = \frac{ab\ V^b}{D} \tag{21}$$

By using numerical tests for a unit-width channel, the numerical model celerity c_n and the theoretical celerity c_t has the following relation

$$c_n = 2.33[(1-\lambda)\ c_t]^{0.96} \tag{22}$$

Substituting Eqs. 19 and 21 into Eq. 22 yields

$$c_n = 2.33\ \left(\frac{ab\ V^b}{D}\right)^{0.96} \tag{23}$$

The time scaling ratio between the prototype and model sediment wave movement is

$$\frac{t_p}{t_m} = \frac{x_p/c_{np}}{x_m/c_{nm}} = \frac{x_p}{x_m}\ \frac{c_{nm}}{c_{np}} \tag{24}$$

in which

$$\frac{c_{nm}}{c_{np}} = \left(\frac{b_m}{b_p}\right)^{0.96} \left(\frac{a_m}{a_p}\right)^{0.96} \left(\frac{V_m^{\ b}}{V_p^{\ b}}\right)^{0.96} \left(\frac{D_p}{D_m}\right)^{0.96} \tag{25}$$

Substituting Eqs. 17 and 18 into Eqs. 24 and 25 to determine the time scaling ratio using d_{50} as a representative particle size:

$$\frac{c_{nm}}{c_{np}} = 392\ \frac{V_m^{\ 4.35}}{V_p^{\ 4.45}} \tag{26}$$

$$\frac{t_p}{t_m} = 175\ \text{x}\ 392\ \frac{V_m^{\ 4.35}}{V_p^{\ 4.45}} \tag{27}$$

A range of prototype velocity from 5 to 20 fps (corresponding to model velocity range from 0.85 to 3.38 fps) yields a range of time scaling ratio between 22 to 25. A constant time ratio of 24 was selected to convert the prototype hydrograph to the model hydrograph for operating the movable-bed model. A similar time ratio was obtained when the sediment continuity equation was applied to two neighboring reaches upstream

of and within the constriction area.

II.5. Determination of Levee Slope for the Movable Boundary Model

The prototype levee slope has a vertical to horizontal slope of 1 to 2. By using a 1:5 vertical to horizontal distortion, the resultant model levee slope was increased to 1 to 0.4 for the fixed-bed model. It is necessary to reduce this slope in the movable-boundary model to obtain required levee stability, which introduces an additional degree of distortion. An attempt was made to determine a model levee slope to achieve comparable levee stability in the model using tractive force theory and critical moment theory. However, it is not known how these changes affect velocity, stage, erosion and deposition patterns. Further research is required in this field.

The tractive force theory states that the motion of a particle is pending when the force tending to cause its motion (τ_m) equals its resistance to motion (τ_s). Based on the Bureau of Reclamation test, for coarse noncohesive material with sufficient factor of safety

$$\tau_L = 0.4\ d_{75} \tag{28}$$

in which τ_L is the permissible tractive force in lbs/ft^2 on a level bottom and d_{75} is in inches. The permissible tractive force on the side slope

$$\tau_s = K\ \tau_L \tag{29}$$

in which K is the tractive force ratio defined as

$$K = \sqrt{1 - \frac{\sin^2\phi}{\sin^2\theta}} \tag{30}$$

where ϕ is the angle of side slope and θ is the angle of repose of a particle.

In the prototype, the d_{75} is 160 mm which has an angle of repose equal to 42 degrees. The angle of the 1 to 2 side slope is 26.5 degrees.

Therefore from Eqs. 28, 29 and 30

$$\tau_L = 0.4 \times \frac{160}{25.4} = 2.52 \text{ lb/ft}^2 \tag{31}$$

$$K = 0.745 \tag{32}$$

$$\tau_s = K\tau_L = 1.88 \text{ lb/ft}^2 \tag{33}$$

The maximum tractive force on the sloping sides is

$$\tau_m \simeq 0.775 \quad \tau_o = 0.775 \left(\frac{1}{8} f\rho V^2 \right) = 0.0150 V^2 \tag{34}$$

For a state of impending motion of a particle on side slope

$$\tau_s = \tau_m \tag{35}$$

This results in

$$V_{cp} = 11.2 \text{ fps} \tag{36}$$

The corresponding critical velocity which initiates particle motion in the model is

$$V_{cm} = 1.89 \text{ fps} \tag{37}$$

The shear stress corresponding to this velocity on the side slope is

$$\tau_{cm} = 0.775 \quad \tau_{Lm} = 0.0537 \text{ lb/ft}^2 \tag{38}$$

The permissible tractive force on the side slope of model for $(d_{75})_m$ = 4.5 mm is

$$\tau_{sm} = K \tau_{Lm} = K(0.4 \times \frac{4.5}{25.4}) = 0.071 K \tag{39}$$

For a state of impending motion of a particle on side slope in the model

$$\tau_{cm} = \tau_{sm} \tag{40}$$

This results in

$$K = 0.756$$

From Eq. 30,

$$\sin\phi = \sin\theta \sqrt{1-K^2} \tag{41}$$

For a particle of 4.5 mm the angle of repose is about 38 degrees. Substituting this angle into Eq. 41 obtains ϕ = 23.8 degrees. This corresponds to a side slope of 1 to 2.2.

This result indicates that if the levee slope in the model is installed at a slope of 1 to 2.2, its stability would be comparable to that in the prototype. Another approach based on Simons and Steven's critical moment theory (Refer to "Highways in the River Environment Hydraulic and Environmental Design Considerations, Training and Design Manual," by E. V. Richardson, D. B. Simons, S. Karaki, K. Mahmood and M. A. Stevens, Civil Engineering Department, Colorado State University, 1975) provides a similar result. Considering the prototype levee slope and the efforts to reduce the distortion effects, a slope of 1 to 2 is selected for constructing the levee in the model.

III. RIVER MECHANICS FLUME AND STUDY AREA

III.1. Description of River Mechanics Flume

The River Mechanics Flume shown in Fig. 2 is situated next to the 600 acre-feet College Lake, south of Colorado State University Engineering Research Center. It is 39.4 feet wide, 120 feet long (with 109.7 ft usable for channel modeling) and 3 feet high. The building also contains a valve house, a 19.5 ft by 16.5 ft pump house which has a 50 hp recirculating pump installed in it, and a small office area. The water supply to the flume is from College Lake through a 350 hp turbine pump and a 21-inch pipeline. A culvert returns the water pumped into the flume back to College Lake. A secondary circulating system has been implemented for movable bed studies to recirculate sediment. The sediment transported through the movable bed models during experiments is collected by a sediment trap located at the end of the flume and the water-sediment

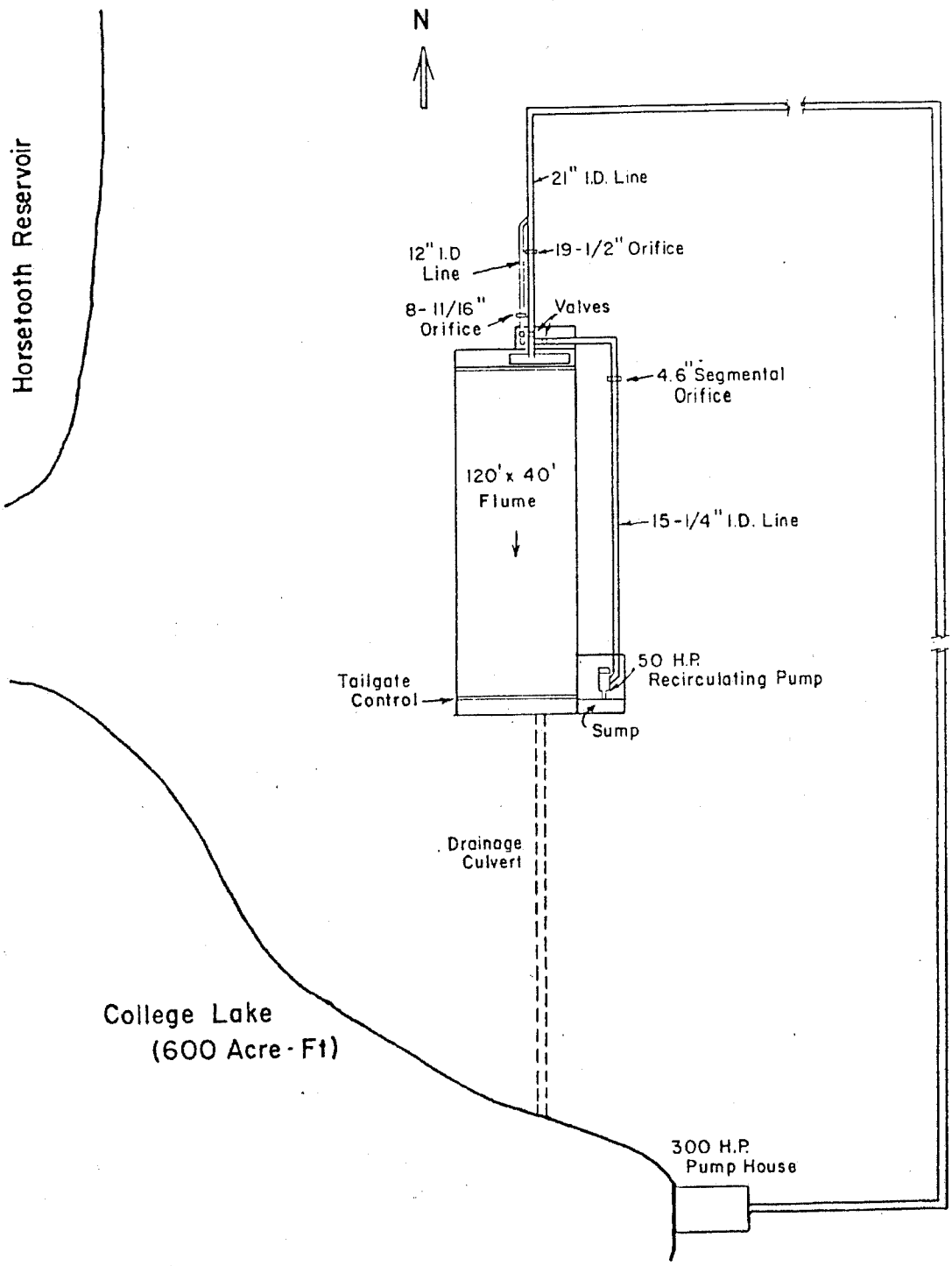

Fig. 2. General Layout of the River Mechanics Flume Testing System, Branch Hydraulics Laboratory

mixture is recirculated by the 50 hp pump and 15 1/4-inch pipeline back into the flume.

The maximum discharge capacity of the main recirculating system is 35 to 40 cfs depending on the fluctuations in College Lake water levels. The secondary system can provide an additional 10 cfs by recirculating some of that discharge whenever higher discharges are needed. With proper piping connections to Horsetooth Reservoir, the system can generate water discharges up to 100 cfs if necessary.

For low discharges, to insure proper discharge measurements by having full-pipe flows, a 12-inch by-pass line to the 21-inch pipeline has been implemented. Flows through different pipelines are controlled by three butterfly valves placed at the ends of them. Discharge measurements are carried out through the use of three orifice plates placed in each one of the pipelines. A differential manometer attached to the pipelines on both sides of the orifice plates measures the head drops across them to a tenth of an inch. The orifice placed in the secondary circuit is selected to be a segmental-type orifice to insure proper operation with a water-sediment mixture passing through it. A more detailed plan view of the flume is given in Fig. 3. A manifold and a porous vertical wall diffuser at the outlet where the water from the pipelines is discharged, are used to introduce a less turbulent flow into the flume. Flow distribution adjustments across the channel can be made by the series of adjustable-height weirs at this location. The surface turbulence at the outlet is suppressed by a series of dissipators manufactured out of wood in the shape of a grill. The water surface elevation adjustments are carried out by the series of stop-logs at the tailwater control.

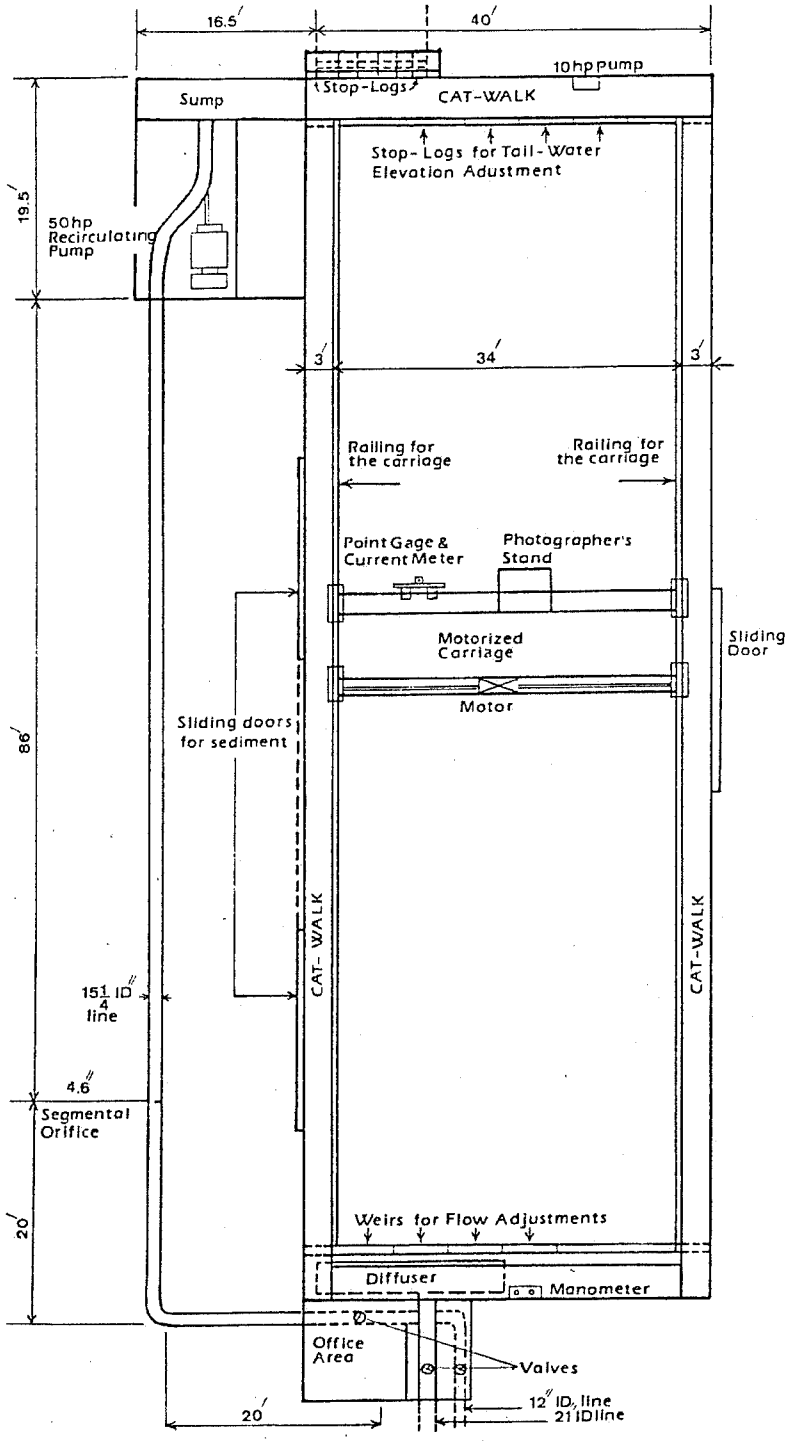

Fig. 3. Detailed Plan View of the River Mechanics Flume

A motorized, 34 ft wide carriage that can move on the railings along the flume is used for carrying the measuring instruments. An overhanging stand mounted on the carriage can be used for flow visualization studies. Sliding doors placed at the sides of the building are accessible to trucks and heavy construciton equipment for quick loading of the desired sediment or other supplies into the flume whenever needed.

III.2. Modeling of Study Area

The Salt River near Sky Harbor International Airport in Phoenix, Arizona was modeled in the River Mechanics Flume. By using model-to-prototype horizontal and vertical length scaling ratios of 1 to 175 and 1 to 35 respectively, the river reach starting from above Priest Road to Interstate I-10 (a length of about 3.7 miles) was modeled. The corresponding model coordinates and the prototype centerline lengths are shown in Fig. 4 and listed in Table 2. Table 2 also lists the model elevation correction to consider the slope change in the model. This is necessary to obtain required roughness element as described in Chapter 2.

Construction of the fixed-bed model follows the procedure:

1) Convert the prototype cross-sectional geometries (provided by HNTB) to the model geometries.

2) Construct the levee lines following the plan provided by HNTB using bricks to about the desired top elevation and applying a cement layer on the bricks to form a 1:0.4 levee slope.

3. Locate the model coordinates of the selected cross sections and lay out the cross-sectional elevations up to about 1 to 2 inches below the desired elevations using the 1/4-inch chips. Bricks were used to stabilize the low flow channel.

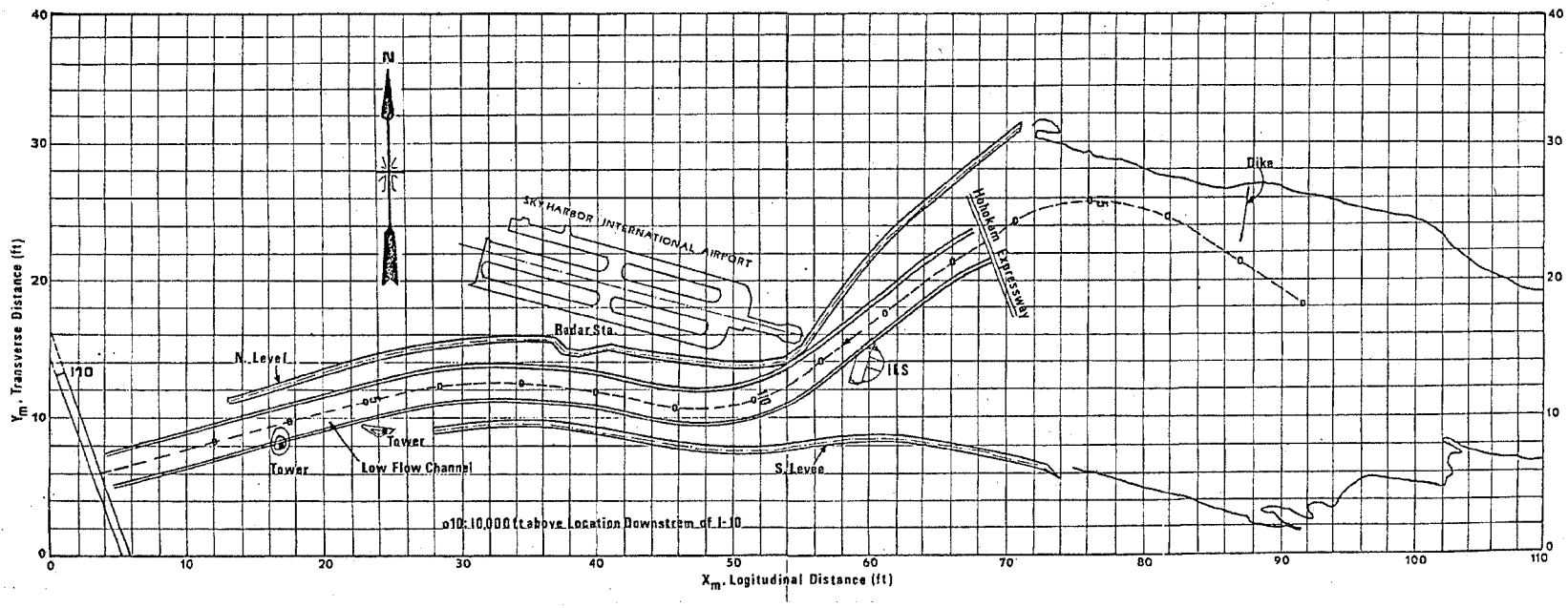

Fig. 4. Model and Prototype Length Coordinates

TABLE 2. Prototype and Model Coordinate Relations

Station	L_p (ft)	ΔZ_m (ft)	Station	L_p (ft)	ΔZ_m (ft)	Station	L_p (ft)	ΔZ_m (ft)
6	1,960	-0.597	37	7,485	-0.383	66	13,040	-0.181
8	2,330	-0.589	38	7,650	-0.376	67	13,255	-0.174
9	2,505	-0.582	39	7,825	-0.370	68	13,470	-0.167
10	2,680	-0.575	40	8,000	-0.363	69	13,685	-0.160
11	2,855	-0.568	41	8,170	-0.356	70	13,900	-0.153
12	3,030	-0.561	42	8,340	-0.349	71	14,085	-0.146
13	3,210	-0.554	43	8,510	-0.342	72	14,270	-0.138
14	3,390	-0.547	44	8,680	-0.335	73	14,450	-0.131
15	3,565	-0.540	45	8,855	-0.328	74	14,630	-0.123
16	3,740	-0.533	46	9,030	-0.321	75	14,805	-0.116
17	3,920	-0.526	47	9,205	-0.314	76	14,980	-0.108
18	4,100	-0.519	48	9,380	-0.307	77	15,155	-0.101
19	4,275	-0.512	49	9,560	-0.300	78	15,330	-0.093
20	4,450	-0.504	50	9,740	-0.293	79	15,515	-0.091
21	4,630	-0.497	51	9,925	-0.286	80	15,700	-0.088
22	4,810	-0.490	52	10,110	-0.279	81	15,875	-0.076
23	4,990	-0.483	53	10,300	-0.272	82	16,050	-0.063
24	5,170	-0.475	54	10,490	-0.265	83	16,235	-0.056
25	5,350	-0.468	55	10,695	-0.258	84	16,420	-0.048
26	5,530	-0.461	56	10,900	-0.251	85	16,625	-0.041
27	5,710	-0.454	57	11,105	-0.244	86	16,830	-0.033
28	5,890	-0.446	58	11,310	-0.237	87	17,035	-0.026
29	6,070	-0.439	59	11,505	-0.230	88	17,240	-0.018
30	6,250	-0.432	60	11,700	-0.223	89	17,460	-0.011
31	6,425	-0.425	61	11,930	-0.216	90	17,680	-0.004
32	6,600	-0.418	62	12,160	-0.209	91	17,900	-0.003
33	6,775	-0.411	63	12,380	-0.202	92	18,120	-0.010
34	6,950	-0.404	64	12,600	-0.195	93	18,340	0.018
35	7,135	-0.397	65	12,820	-0.188	94	18,560	0.025
36	7,320	-0.390						

L_p = Prototype distance above station 1,000 ft downstream of I-10

ΔZ_m = Model elevation correction due to slope change

4) Cover the chip surface using 1 1/2-inch gravel to the desired elevations. A completed fixed bed model is illustrated in Fig. 5.

Three discharges, 92,000 cfs, 176,000 cfs and 210,000 cfs were tested in the fixed-bed model. The corresponding model discharge and stage conditions are given in Table 3. The model stages at the control station were determined based on the prototype stages at about 50 ft upstream of I-10, provided by Anderson-Nichols for the post-project conditions.

TABLE 3. Model Test Conditions

Prototype		Model	
Discharge (cfs) Q_p	Stage (ft, msl) h_p	Discharge (cfs) Q_m	Stage (ft) h_m*
92,000	1,094.8	2.54	1.61
176,000	1,101.1	4.86	1.79
210,000	1,102.8	5.80	1.84

* $h_m = (h_p - 1{,}060)/35 + \Delta Z_m$

After the completion of the fixed-bed model tests, the gravel and bricks were removed. The 1/4-inch chips were used to fill these areas and to form the levee. The model levee slope was molded to a 1:2 slope. Sections of levees were protected by 1 1/2-inch gravel according to HNTB's plan.

III.3. Instrumentation

The major variables measured during the model tests include water discharge, velocity, and water surface and bed surface elevation. Stop

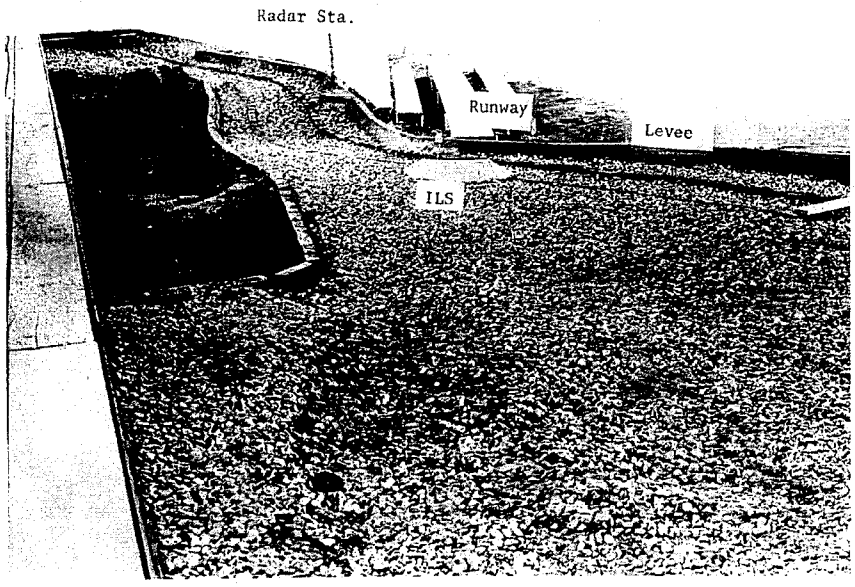

(a) Dry Channel

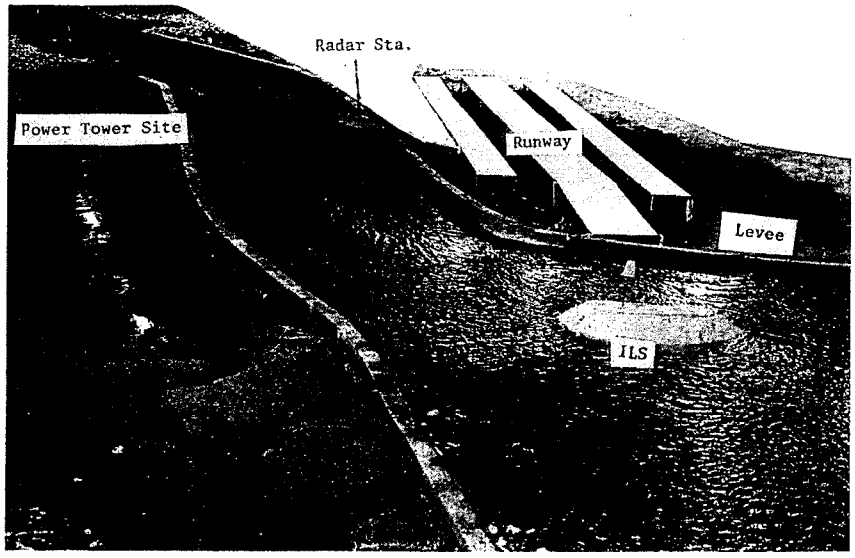

(b) Q = 92,000 cfs

Fig. 5. Photographs Showing the Fixed-Bed Model

logs are used to control stages at the control station immediately upstream of I-10.

The water discharge is measured using a 8 11/16-inch orifice installed in the 12-inch bypass line. This orifice has been calibrated using the Hydraulics Laboratory Pipe flow calibration system. The calibration relation is

$$Q = 2.377\ (\Delta h)^{0.49} \tag{42}$$

in which Q is the discharge in cfs and Δh is the head loss across the orifice in feet.

The velocity is measured using a 1-inch ott meter. The rating relation is

$$v = 0.3395\ n + 0.125 \tag{43}$$

in which n is the number of revolutions per second, and v is the point-velocity in fps. Flow direction is also measured by tying a string to the tip of point gage to indicate direction and measuring the angle of flow with respect to the carriage baseline. The water surface and bed surface elevations are measured using a point gage and periodically checked using a transit.

IV. RESULTS OF FIXED-BED MODEL TESTS

Three discharges, 92,000 cfs, 176,000 cfs, and 210,000 cfs, were tested in the fixed-bed model. During earlier tests, some adjustments have been made to improve the model performance. These include:

1) The water discharge entering the flume was originally measured by using the 19 1/2-inch orifice in the 21-inch line. It was later changed to use the 8 11/16-inch orifice in the 12-inch bypass line to increase the accuracy for measuring low discharges.

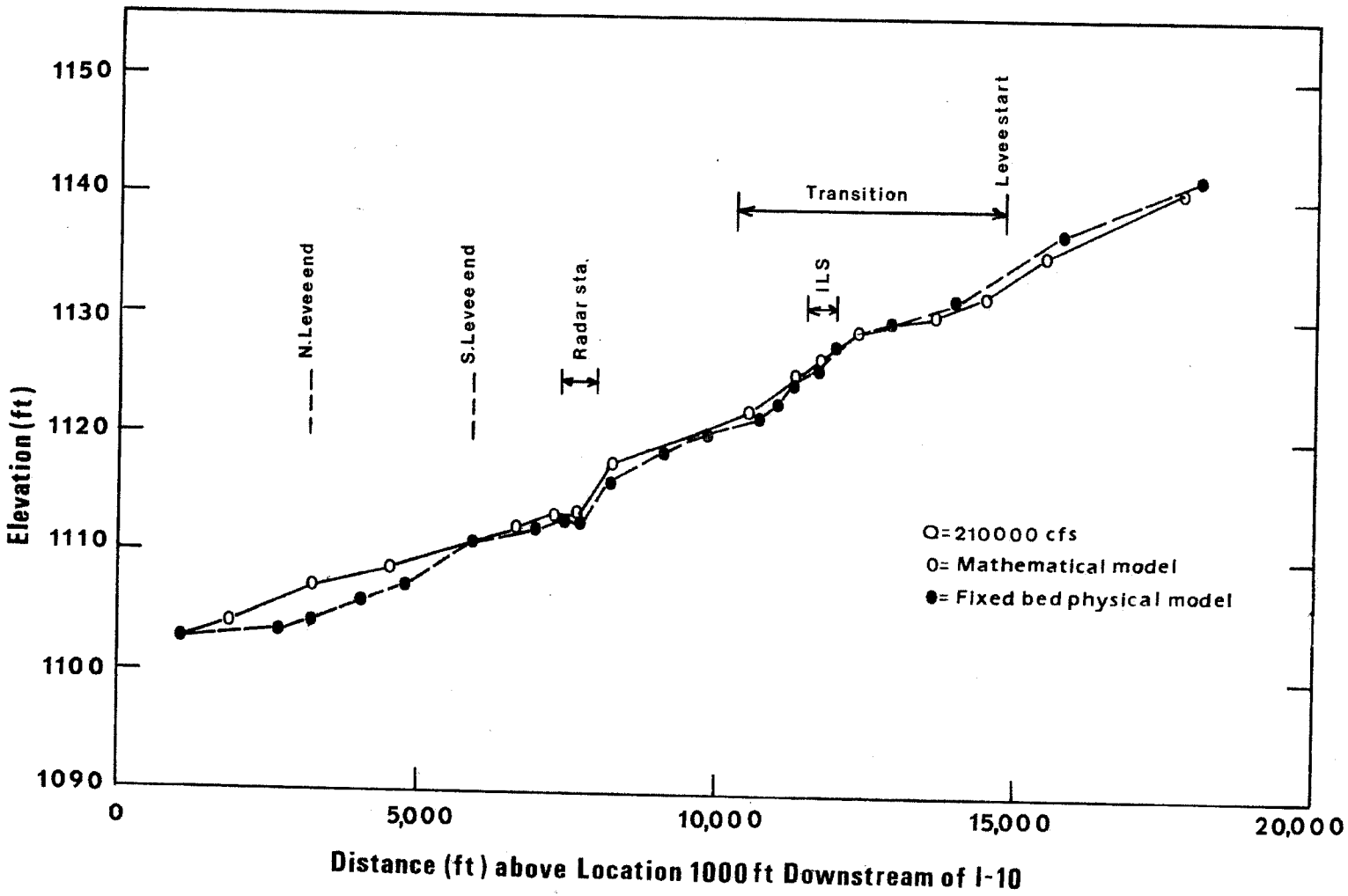

Fig. 8. Comparison between Average Stages of Fixed-bed Physical Model and Mathematical Model Stages at Q = 210,000 cfs

downstream of the south levee. The major factor contributing to these differences could be the difference in the cross-sectional geometry in this reach of river. The cross-sectional geometry utilized by Anderson-Nichols to determine stages in the mathematical model considers the south levee ended at the same station as the north levee while the physical model terminates the south levee at about 2,600 ft upstream of the north levee end.

IV.2. Velocity Distributions in the Fixed-Bed Physical Model

Flow velocities including directions were measured when running the fixed-bed physical model at Q_p = 92,000 cfs, 176,000 cfs and 210,000 cfs. Most of the velocities were measured at about 0.6 depth above the riverbed. Spot checks showed these velocities were about the average velocities at verticals. Figures 9, 10 and 11 show the measured velocities in fps for the three discharge conditions respectively. In general, velocity varies significantly in longitudinal direction as well as transverse direction. Maximum velocities usually occur in the constriction reach at the Radar Station. These velocities provide a good indication of levee stability as will be discussed in Sec. 4.3. The low flow channel if remaining stable has the capability to guide the main flow current along its channel alignment. This effect reduces with the increase in discharge.

The proportion of flow discharge passing through the section south of ILS increases with discharge. As shown in Fig. 12, the dividing ratio of discharge increases from 31 percent for 92,000 cfs to 37 percent for 210,000 cfs. From the discussions with Engineers for the City of Phoenix and HNTB, there is a concern that the flow through the channel south of ILS would increase with time as future major floods could open

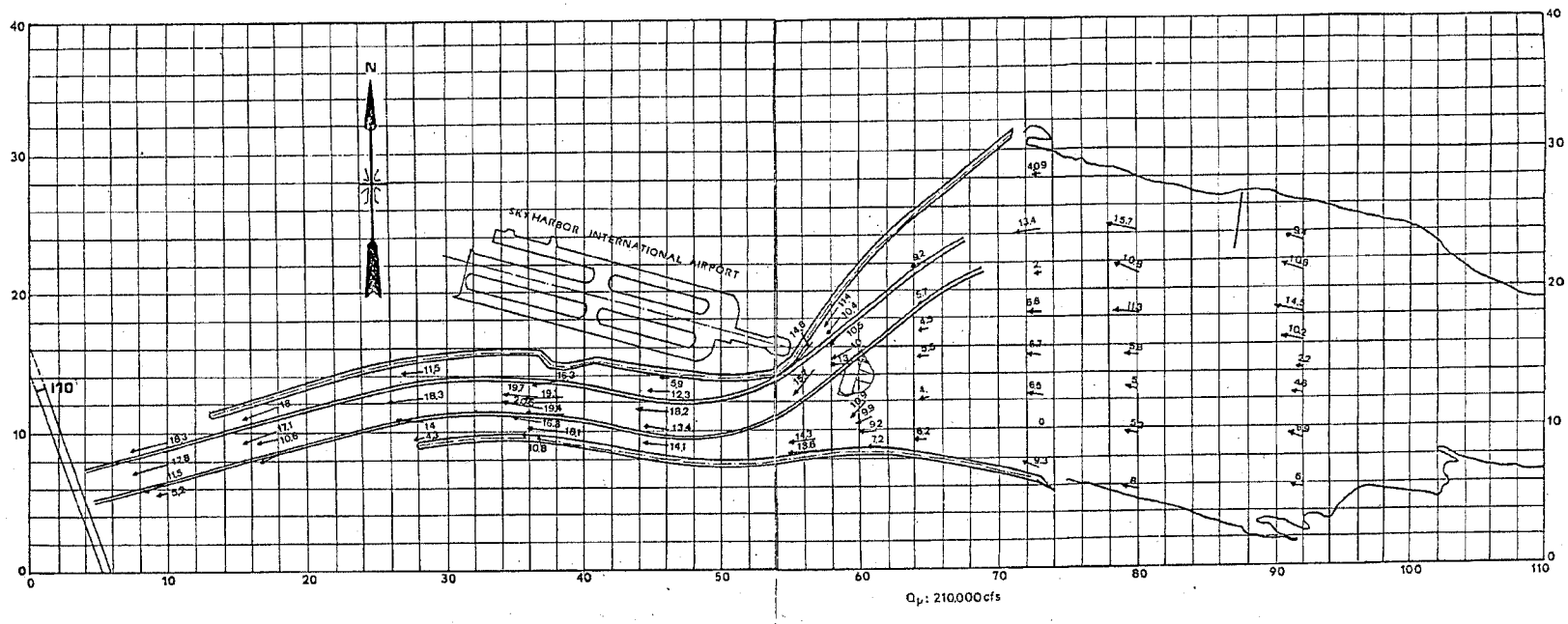

Fig. 11. Velocity Distributions in the Fixed-bed Model at 210,000 cfs

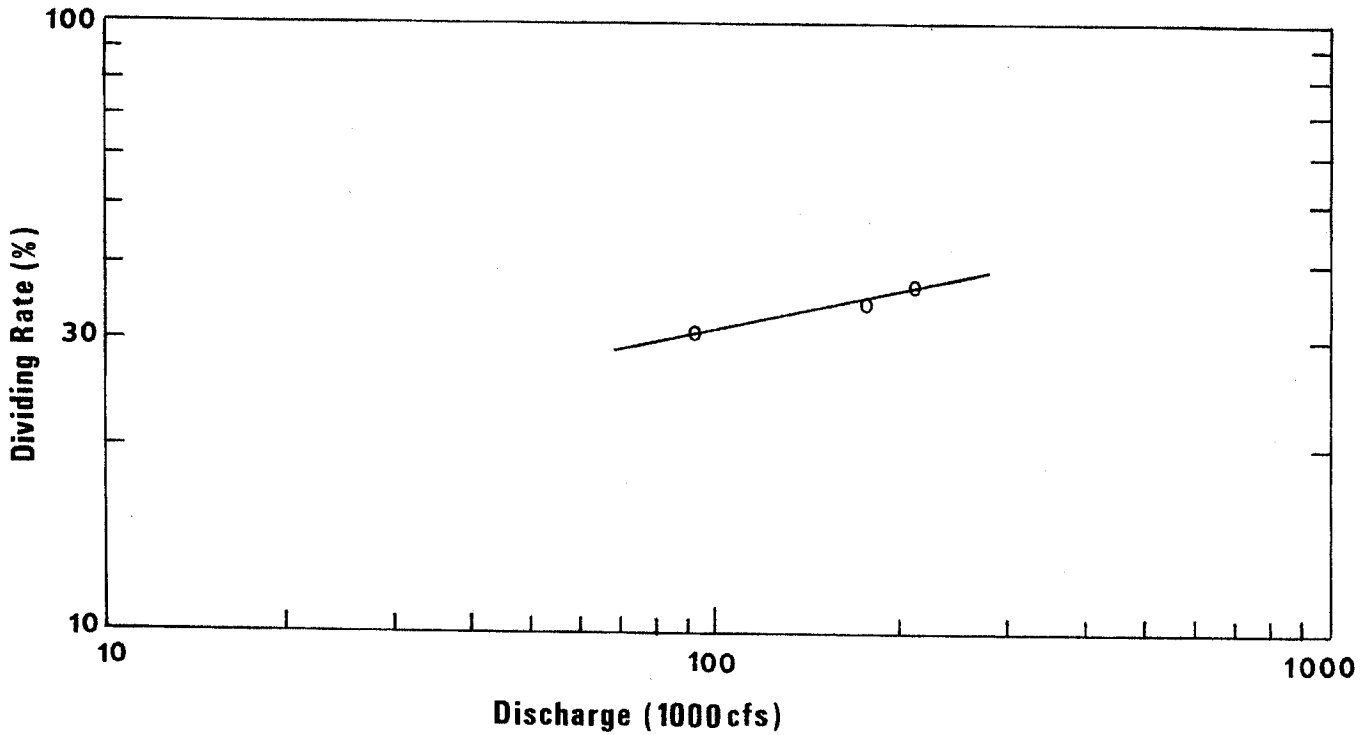

Fig. 12. Flow Division around the ILS

up the south channel. This increase could in turn change the area of attacks and make the protection of levee lines more difficult. After examining the river patterns including the upstream undivided river reach, we think the possible increase in the flow discharge through the channel south of ILS would be limited.

Another concern is that the chute channel near the south bank upstream of the channelized reach is deeper than that in the channelized reach. Major flood could cut into this south channel reach to increase the discharge proportion. To study this problem, a channel was excavated starting at about Station 74 near the south levee and entered the low flow channel at about Station 52. The dimensions of this excavated channel were about 260 ft wide and 6.5 ft deep. The velocities and stages at selected stations were then measured. It was found that with this increase in flow area, the discharge proportion through the south channel increased from 37 percent to 43 percent. The local velocity in the enlarged channel section increased from 7.2 fps to 9.6 fps at Station 61. The effects of these changes in flow diversion become negligible downstream of Station 50. A better idea of these types of changes can be obtained through the movable-bed model studies.

IV.3. Preliminary Evaluation of Channelization System

Based on the fixed-bed model results, some preliminary evaluations of the proposed channelization system can be drawn.

1) With the very high velocities in the low-flow channel, significant damage to this channel would occur during passage of major floods.

2) The levee freeboard in the channel reach downstream of Station 60 would be larger than 3 ft at Q_p = 210,000 cfs (100 year flood) as shown in Table 7. However, the south levee upstream of Station 60

should be raised 1 to 2 ft to obtain 3-ft freeboard, while the levees below Station 55 can be lowered by about 1 to 7 ft.

3) The levee protection plan proposed by HNTB is not very adequate after comparing the velocity near the levee lines with the critical velocity impending motion to a particle on side slope (c_{cp} = 11.2 fps, derived in Section 2.4). Figure 13 shows the proposed levee protection for the design discharge of 92,000 cfs and 210,000 cfs compared with that suggested by HNTB. These proposed levee protection systems based on the fixed-bed model results were later evaluated in the movable-bed model and found to be reasonable, except that the protection of the upper north levee should be extended to Station 69.

TABLE 7. Freeboard for Q = 210,000 cfs

Station	L_p (ft)	North Levee (ft)		South Levee (ft)	
		Levee Height	Freeboard	Levee Height	Freeboard
13	3,210	1,114.5	10.7	-	-
18	4,100	1,115.4	9.9	-	-
22	4,810	1,116.2	7.7	-	-
28.3	5,940	1,117.2	6.1	1,117.0	6.1
34	6,950	1,118.7	6.6	1,119.0	7.1
37	7,485	1,120.7	8.2	1,120.9	7.7
38.5	7,730	1,121.1	10.0	1,121.4	8.8
41	8,170	1,121.8	5.6	1,122.2	5.8
46.2	9,080	1,123.3	5.5	1,123.5	4.0
50.2	9,780	1,124.6	5.9	1,124.6	3.7
55	10,690	1,126.4	5.7	1,125.7	3.5
56.7	11,020	1,127.7	3.9	1,126.7	3.7
58.1	11,310	1,129.7	3.7	1,127.7	3.1
60	11,700	1,130.5	3.4	1,128.9	2.9
61	11,940	1,131.0	3.6	1,129.6	2.6
65	12,820	1,132.8	2.8	1,130.7	1.2
71	14,080	1,134.8	3.7	1,132.8	2.2

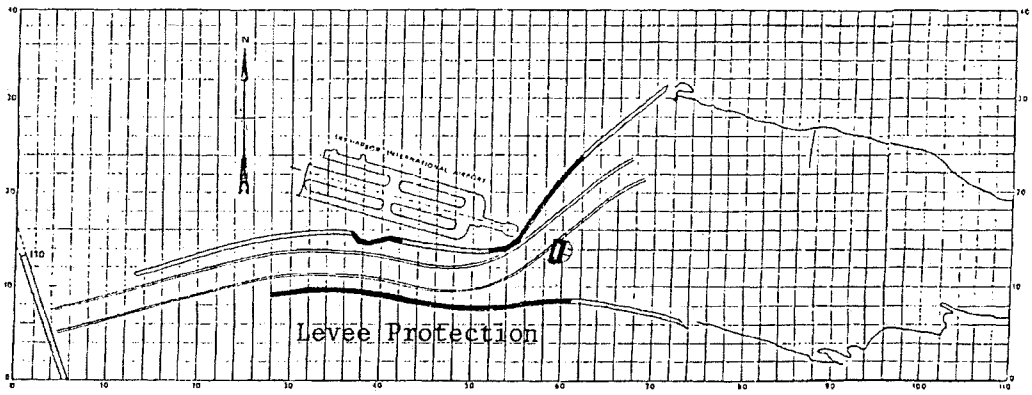

(a) HNTB Levee Protection Plan

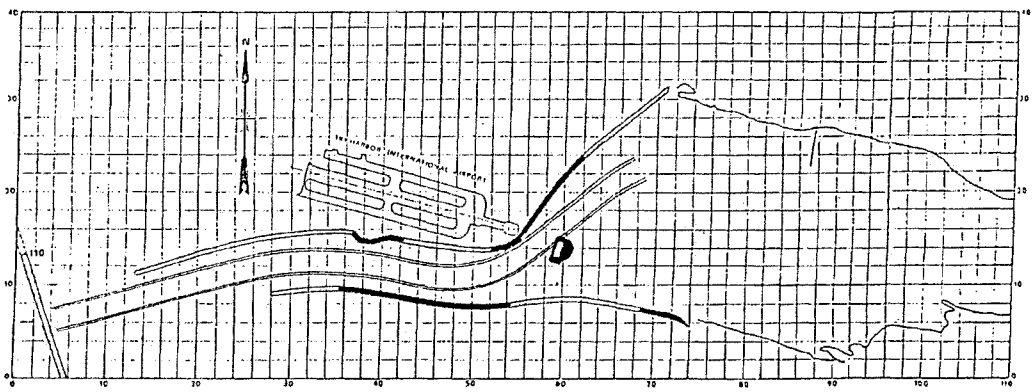

(b) Preliminary Modification at Q = 92,000 cfs

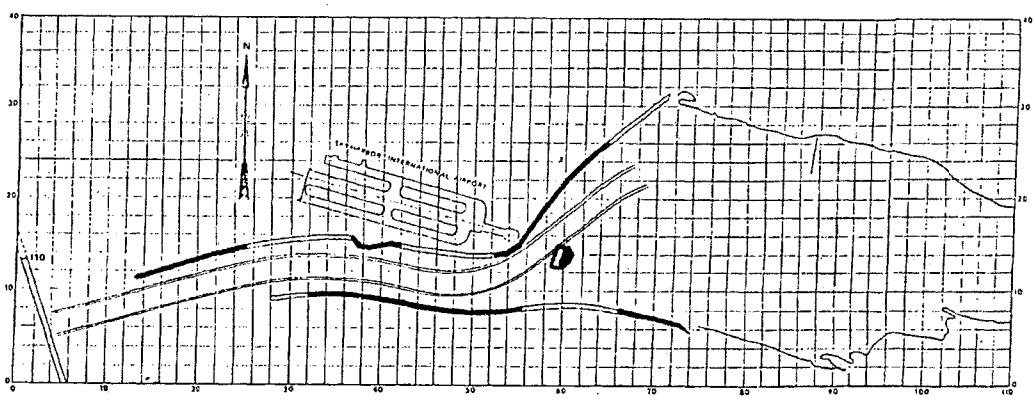

(c) Preliminary Modification at Q = 210,000 cfs

Fig. 13. Preliminary Review of the HNTB Levee Protection Plan and Possible Modifications

V. MOVABLE-BED MODEL TESTS

The movable-bed model of the Salt River Channelization Project at Sky Harbor International Airport, Phoenix, Arizona, was constructed and operated to evaluate the adequacy of the channelization project. In this chapter, the construction and operation of the movable-bed model is described. The test results of the movable-bed model and their comparisons with the fixed-bed model are presented.

V.1. Construction of the Movable-Bed Model

In the fixed-bed model, the 1 1/2 inch gravel was utilized to cover the 1/4-inch chips to form the fixed bed. After the completion of the fixed-bed model tests, the gravel layer and brick levees were removed. The 1/4-inch chips (see Fig. 1 for the size distribution) were used to fill these areas and to form the levee. The model levee slope was molded to a 1:2 slope as discussed in Section 2.5. Sections of levees were protected by 1 1/2-inch gravel according to HNTB's plan.

Because of the changes in bank and levee slopes from 1:0.4 to 1:2, some distortions in cross sections are required. Figure 14 shows the changes in the shape of a typical cross section and the cross-sectional shape adjacent to Stations 55 and 60 where the levee slope is connecting the low flow channel. As shown in Fig. 14, the changes in cross-sectional shapes are usually relatively minor. Figures 15 and 16 show photographs of the completed movable-bed model. For computing the changes in bed elevations in the movable-bed model, the initial bed elevations of the model are given in Fig. 17. To obtain the true bed elevations, the numbers in Fig. 17 should be increased by 1,100 ft when the number is smaller than 30 and should be increased by 1,000 ft when it is larger than 80.

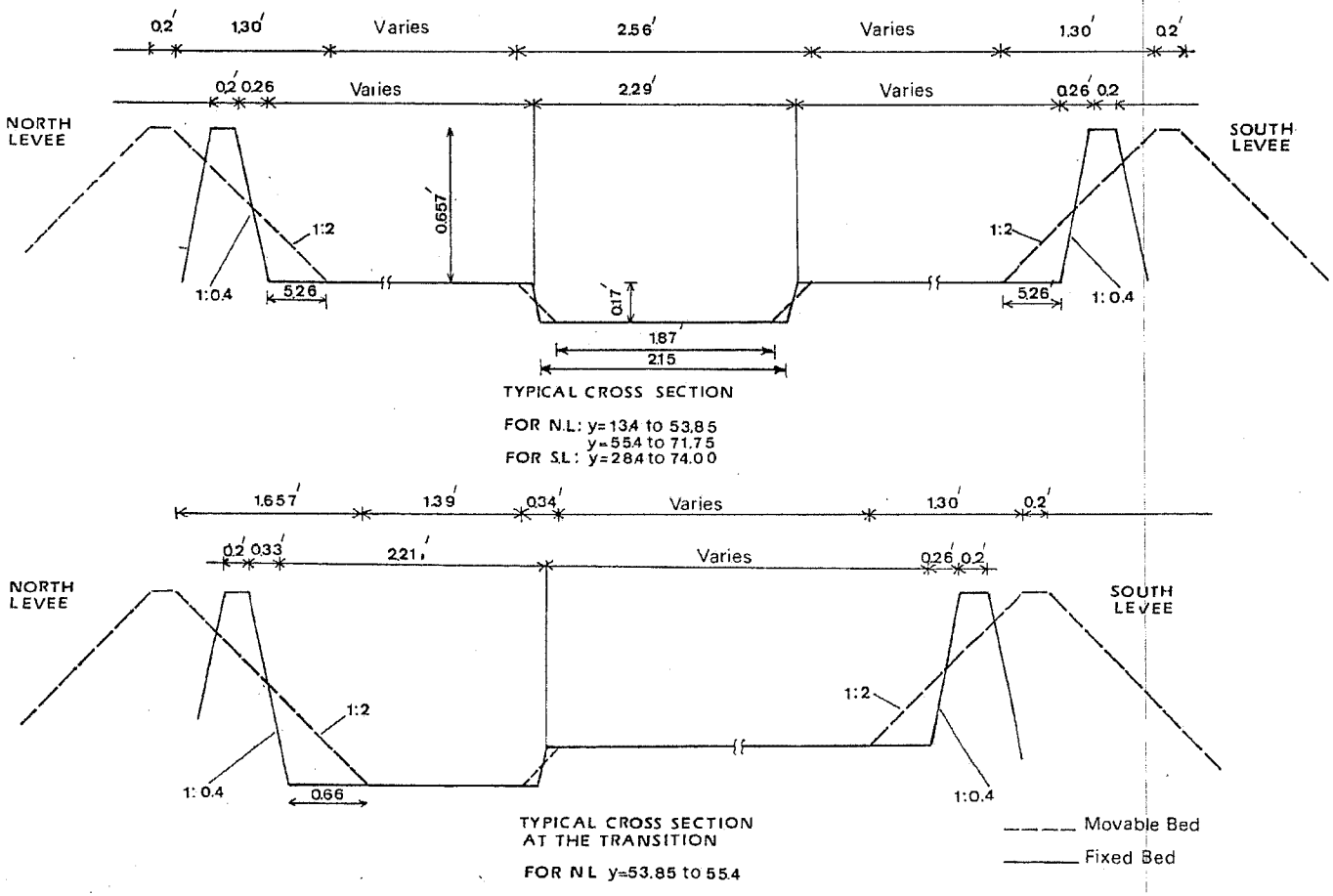

Fig. 14. Modified Cross-Sectional Shapes in the Movable-Bed Model

Fig. 15. Photo of the Movable-Bed Model

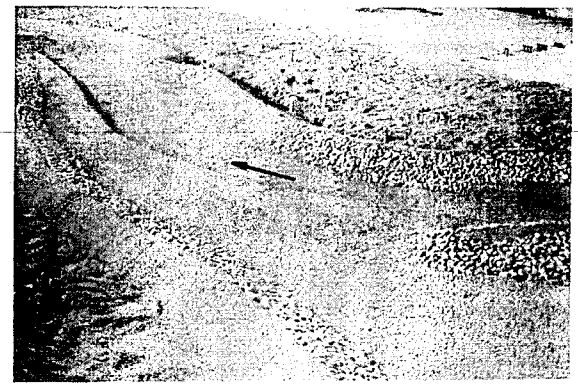

(a) Looking towards the radar station from the ILS

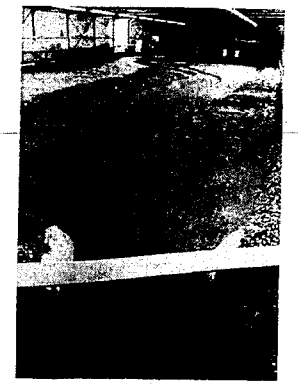

(b) Looking upstream from I-10

(c) Looking upstream towards the ILS

(d) Looking downstream from the radar station

Fig. 16. Various Views of the Movable-Bed Model

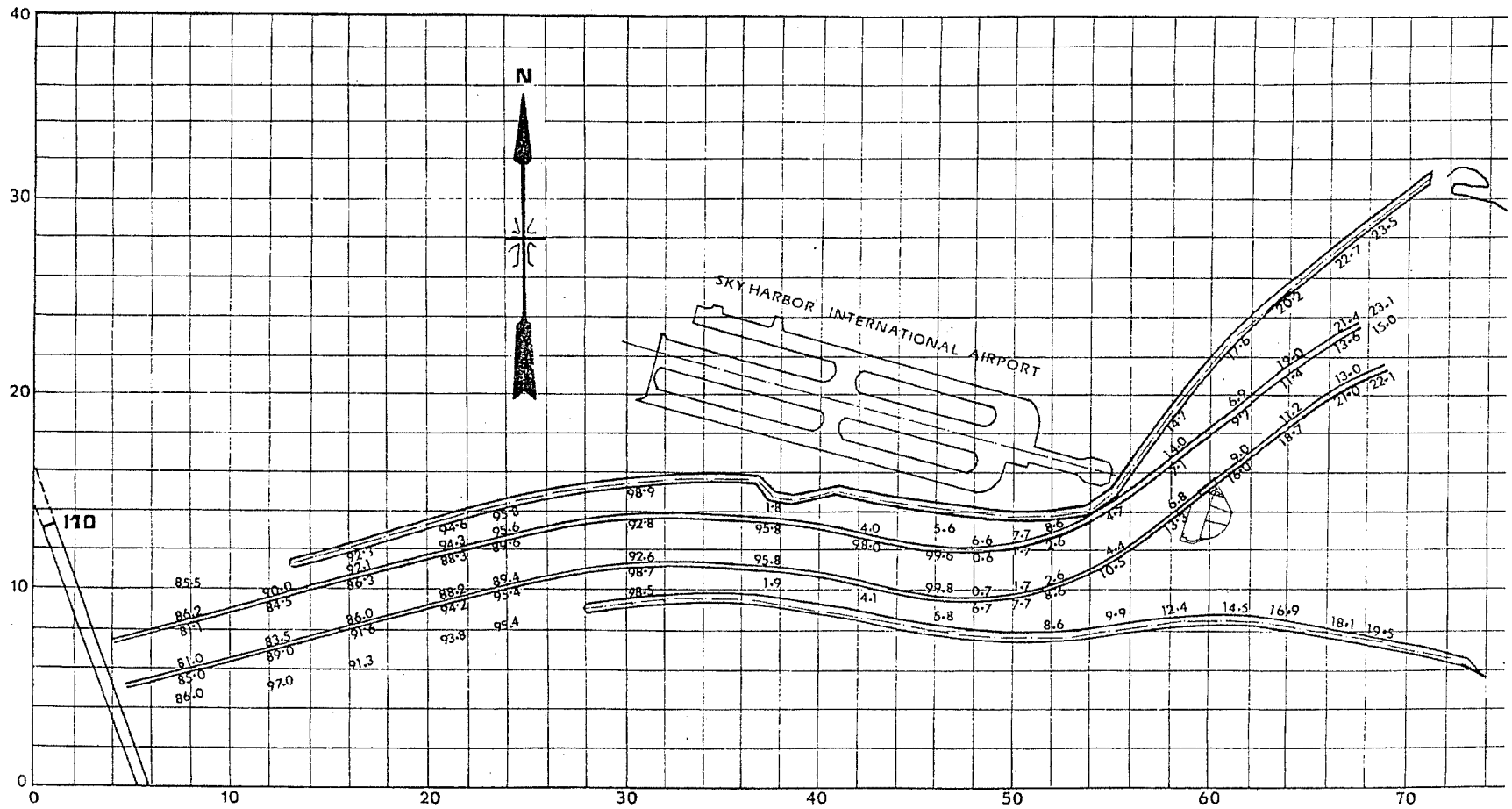

Fig. 17. The Initial Bed Elevations in the Movable-Bed Model

V.2. Operation of the Movable-Bed Model

A standardized hydrograph was developed by HNTB (see Fig. 18). This hydrograph was utilized to synthesize two different hydrographs, i.e.:

1) 92,000-cfs hydrograph - multiplying the discharges in the standardized hydrograph by 92,000 to obtain a peak discharge of 92,000 cfs.

2) 210,000 cfs hydrograph - multiplying the discharges in the standardized hydrograph by 210,000 to obtain a peak discharge of 210,000 cfs.

To run these hydrographs through the movable-bed model, the hydrographs were approximated by step hydrographs as shown in Fig. 18. Considering a model-to-prototype time scaling ratio of 1 to 24 as discussed in Section 2.4 and neglecting smaller discharge steps during which sediment discharges would be small, the model step discharges, time durations and corresponding water surface elevations at immediately upstream of I-10 are listed in Table 8. The water surface elevations were obtained based on the rating curve utilized by SLA. This rating curve provides essentially the same stages as those given by Anderson-Nichols.

The model operating procedure and the data collection program involve:

1) Routing the 92,000 cfs hydrograph through the model.

2) During the run, velocities at Stations 186+00, 55, 46, 38.5, and 19 were collected when there was sufficient time. In addition, stability of levees were observed and protection of levees were provided wherever it was necessary.

3) After routing the first 92,000-cfs hydrograph, the bed elevations were measured in detail.

4) Without reforming the bed profile, the 92,000 cfs hydrograph was routed through the model for the second time. The same data described in Steps 2 and 3 were collected to study cumulative effects of subsequent floods.

5) The bed profile was then re-molded to the initial condition. A 210,000 cfs hydrograph was routed through the model.

TABLE 8. Step Discharges, Durations and Stages in the Movable-Bed Model

Prototype			Model		
Time (day)	Discharge (cfs)	Stage (ft, msl)	Time (hours)	Discharge (cfs)	Stage (ft)
I. 92,000 cfs Hydrograph					
2-3	27,600	1,088.2	0-1	0.76	1.43
3-4	69,900	1,093.4	1-2	1.93	1.57
4-4.5	92,000	1,095.2	2.2.5	2.54	1.63
4.5-5	72,700	1,093.6	2.5-3	2.01	1.58
5-6	27,600	1,088.2	3-4	0.76	1.43
II. 210,000 cfs Hydrograph					
1-2	23,100	1,087.3	0.1	0.64	1.40
2-3	63,000	1,092.7	1-2	1.74	1.55
3-4	160,000	1,100.0	2-3	4.42	1.76
4-4.5	210,000	1,102.8	3.3.5	5.80	1.84
4.5-5	166,000	1,100.4	3.5-4	4.58	1.77
5-6	63,000	1,092.7	4-5	1.74	1.55
6-7	44,100	1,090.6	5-6	1.21	1.49
7-8	23,100	1,087.4	6-7	0.64	1.40

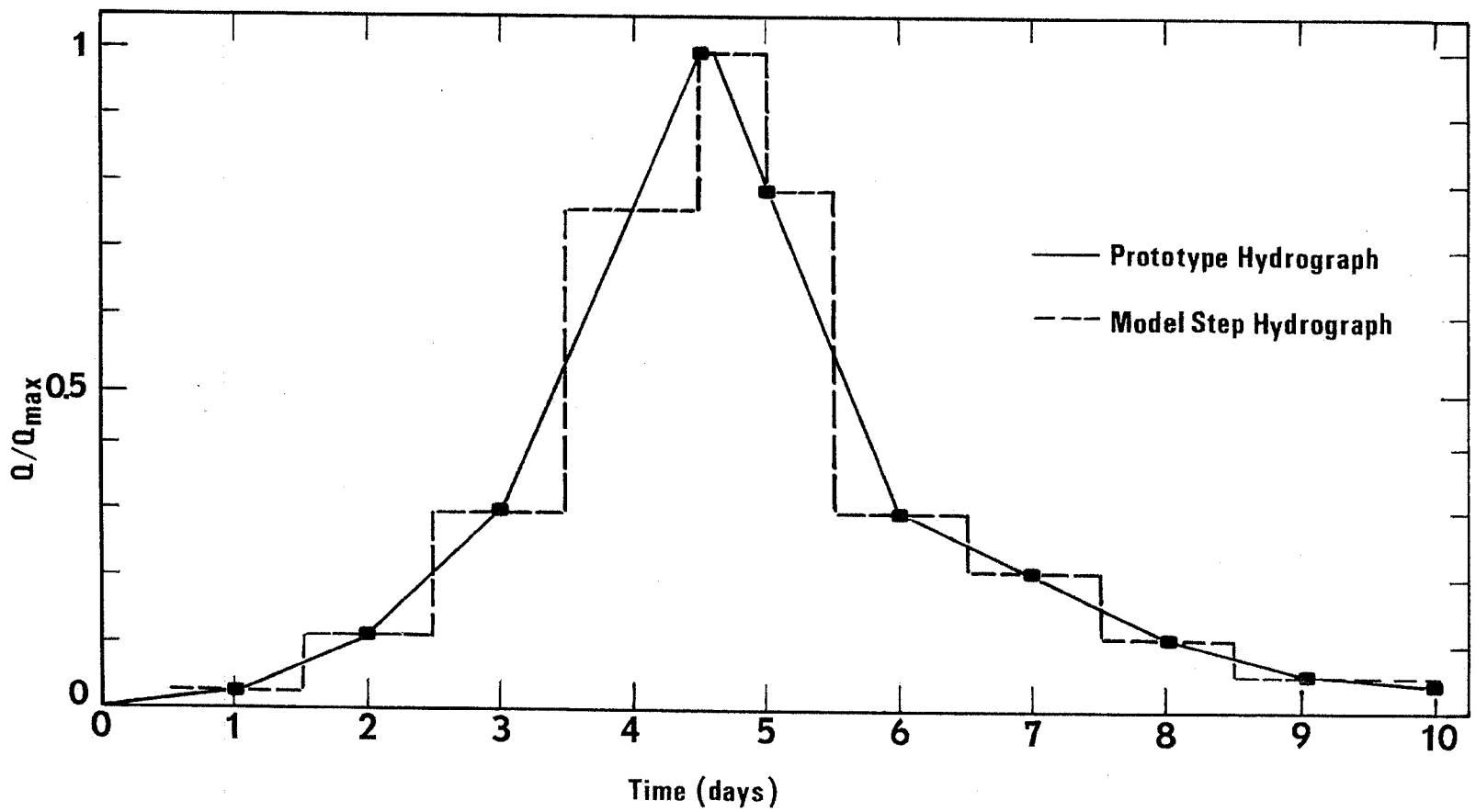

Fig. 18. Standardized Discharge Hydrograph

6) Velocities were measured at the stations given in Step 2.

7) At the end of the rising limb, flow was stopped and the flume was drained to measure the bed elevations.

8) The bed elevations were measured again after routing the entire 210,000 cfs hydrograph.

Filling and draining of water were done at a slow rate during the initiation and completion of model runs, to minimize artificial disturbance.

V.3. Bed-Elevation Changes

Bed elevations changed significantly during passages of hydrographs especially at high flow. Figures 19 and 20 show photographs of the bed profiles in the movable-bed model after routing the first and second 92,000 cfs hydrographs respectively. As can be seen in these photos, subsequent floods would not change the general erosion and deposition patterns, but they would smooth the bed profiles. These changes can also be clearly seen in the bed contour plots based on the measured bed elevations as shown in Figs. 21 and 22.

As observed in the model tests, The main flow impinged on the north levee near Station 60, moved along the north levee until the end of transition at Station 54, then separated from the north levee and followed its momentum to attack the south levee near Station 44, and then deflected away to attack the north levee near Station 24. This main flow eroded the riverbed along its path and developed a point bar downstream of transition and upstream of the radar station near the north levee as shown in Figs. 21 and 22. Figures 23 and 24 show the bed elevation changes from the initial values for the first and second 92,000 cfs hydrograph runs, respectively. Figures 25 through 28 show the changes in cross-sectional shapes at Stations 21.5, 37.6, 42.5 and 58.4 after

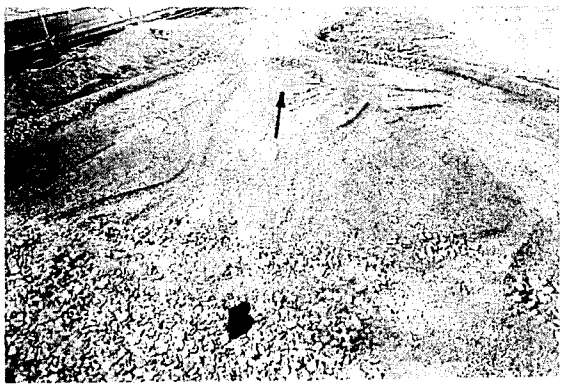

(a) Braided channels formed upstream of the ILS

(b) Extensive erosion occurred along the south levee downstream of transition and in the vicinity of radar station

(c) Bed profile changes upstream of the ILS

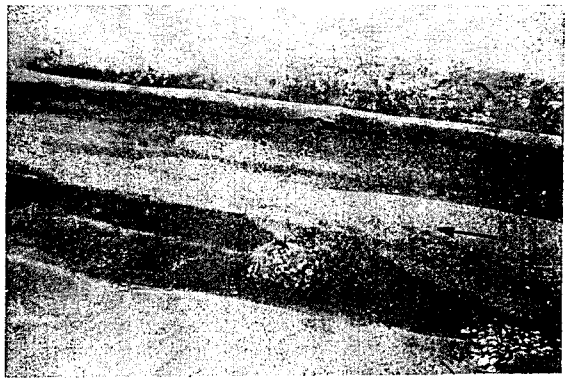

(d) Bed erosion near the lower north levee (top of sticks show the initial bed elevation)

Fig. 19. Photos showing the Bed Surface of the Movable-Bed Model after Routing the First 92,000 cfs Hydrograph

(a) Braided channels formed after the first hydrograph enlarged

(b) Scour hole near the south levee below the ILS elongated and became shallower compared to that after first hydrograph

(c) Erosion near levees and deposition in the low-flow channel at the radar station

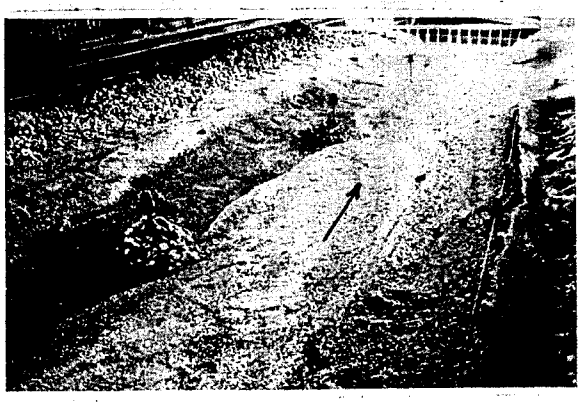

(d) Continuous erosion along the lower north levee

Fig. 20. Photos showing the Bed Surface of the Movable-Bed Model after Routing the Second 92,000 cfs Hydrograph

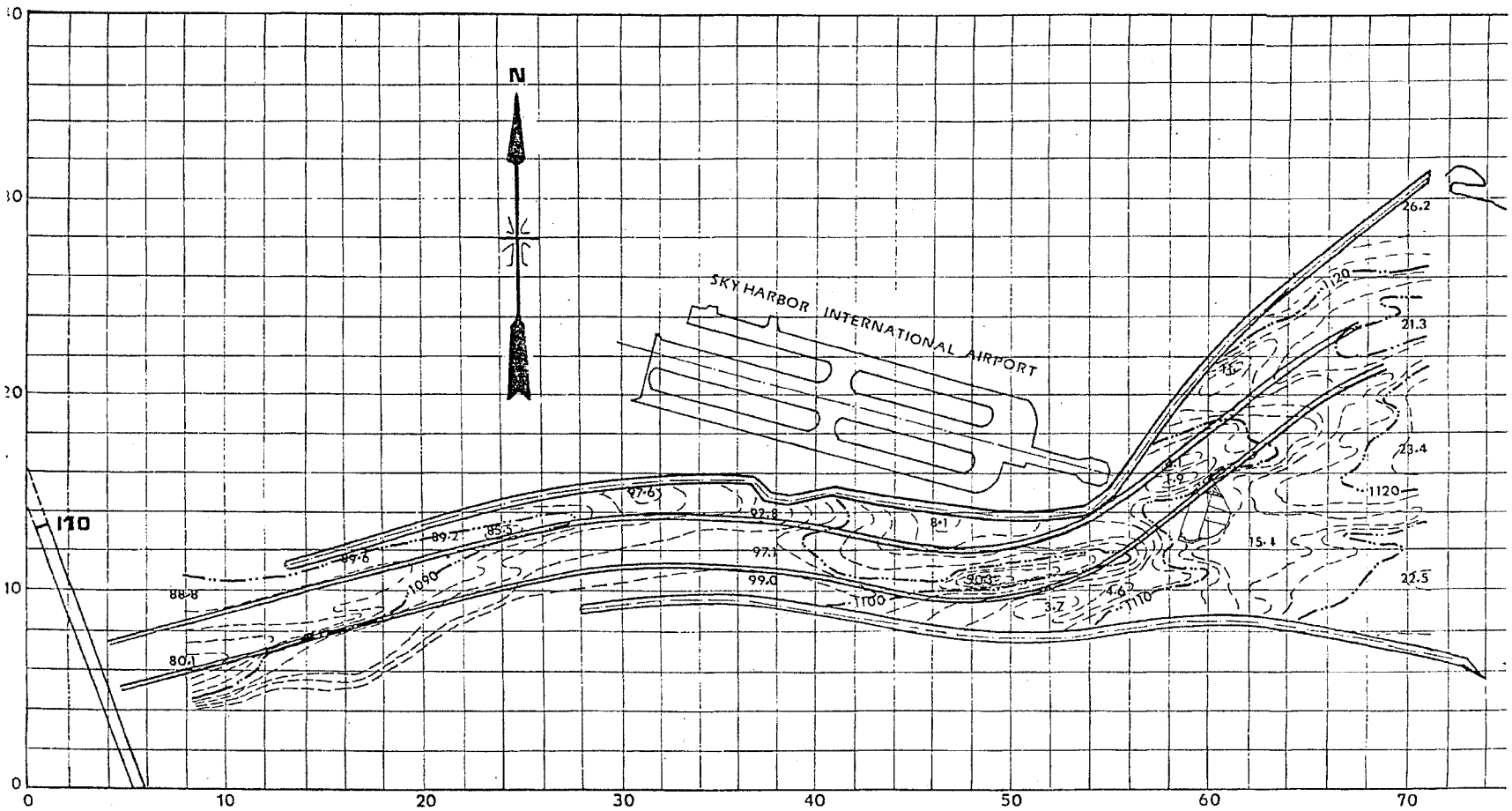

Fig. 21. Bed Contours in the Movable-Bed Model after Routing the First 92,000 cfs Hydrograph

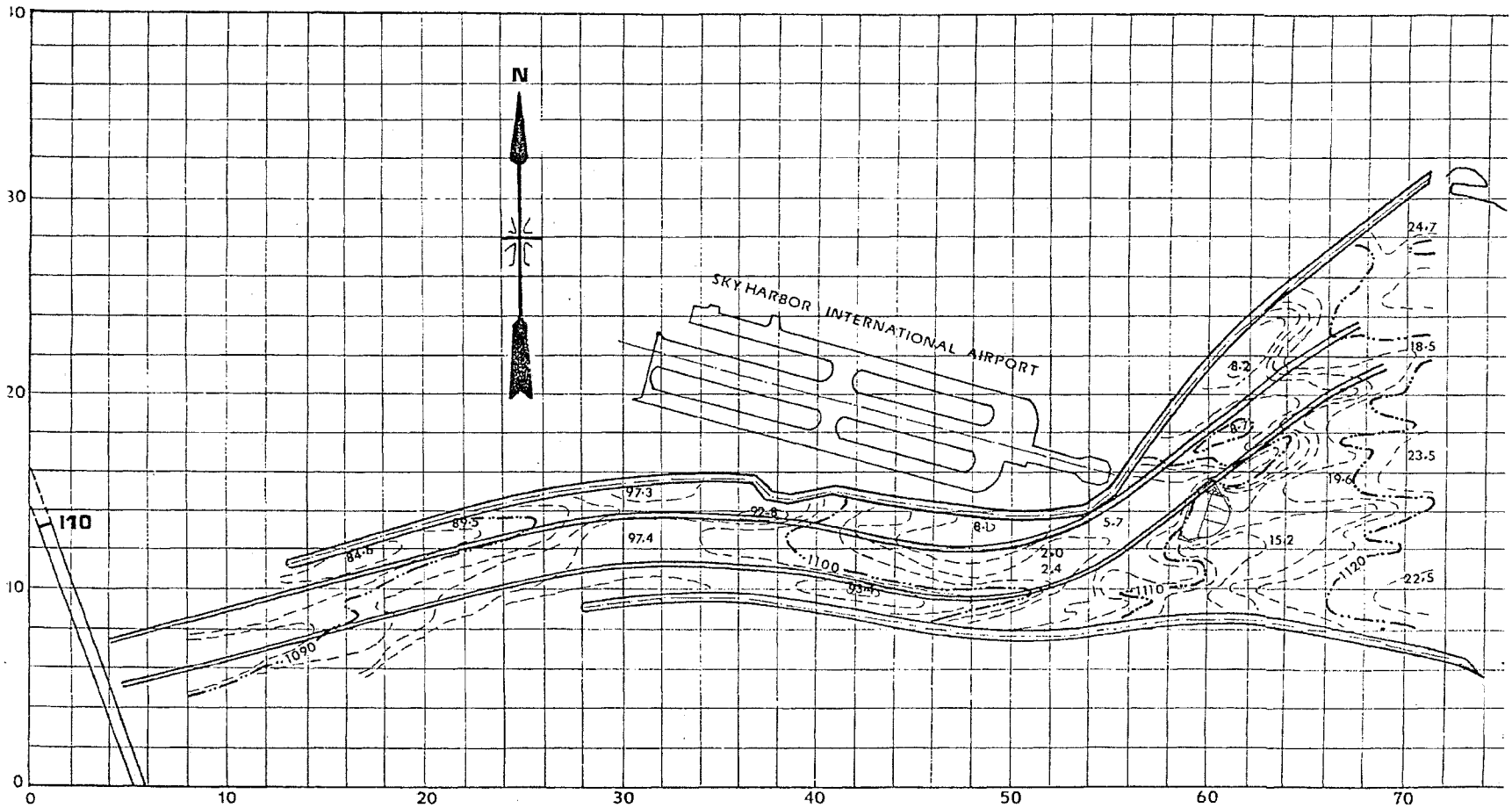

Fig. 22. Bed Contours in the Movable-Bed Model after Routing the Second 92,000 cfs Hydrograph

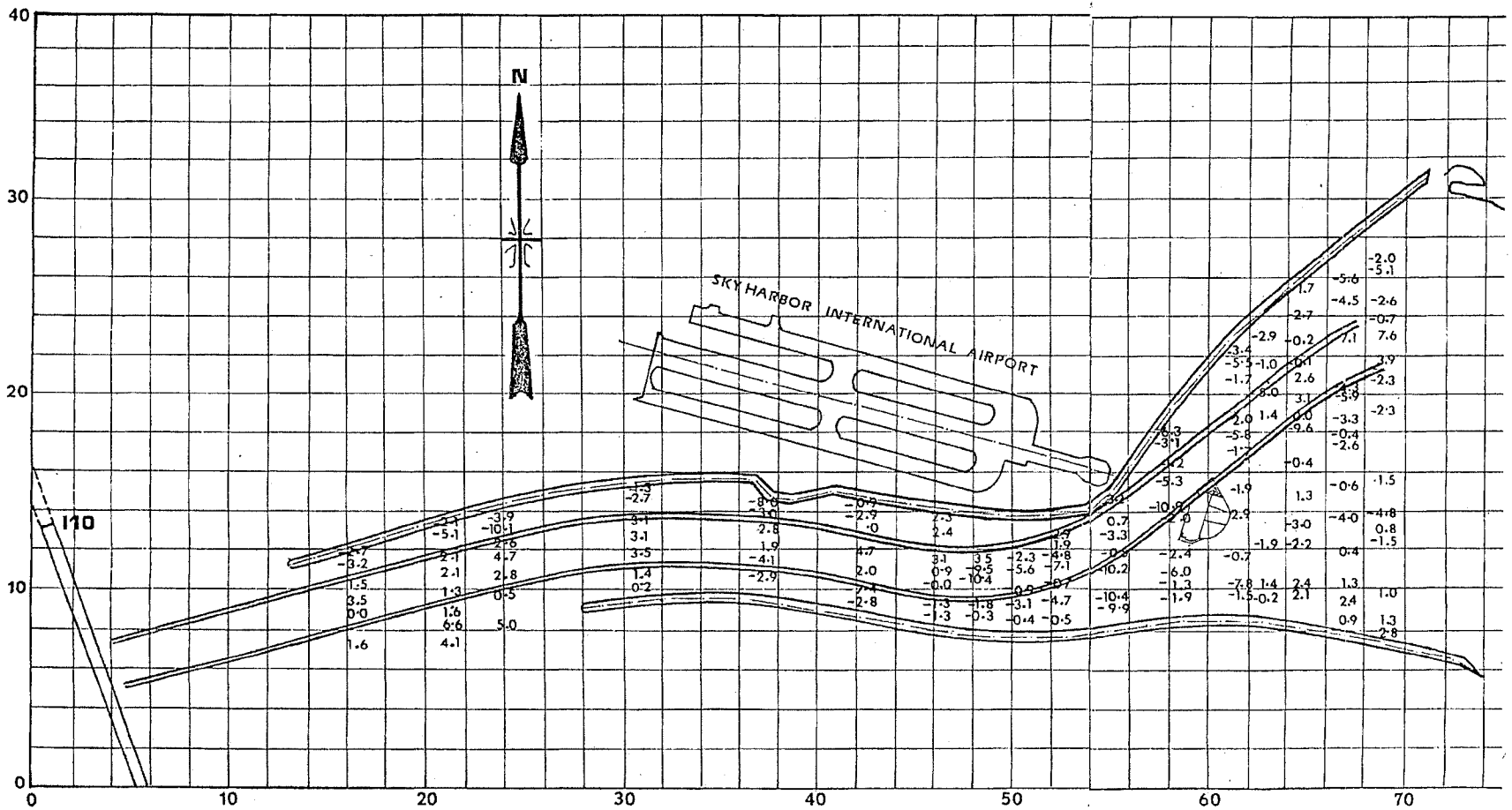

Fig. 23. Bed Elevation Changes from the Initial Values after Routing the First 92,000 cfs Hydrograph

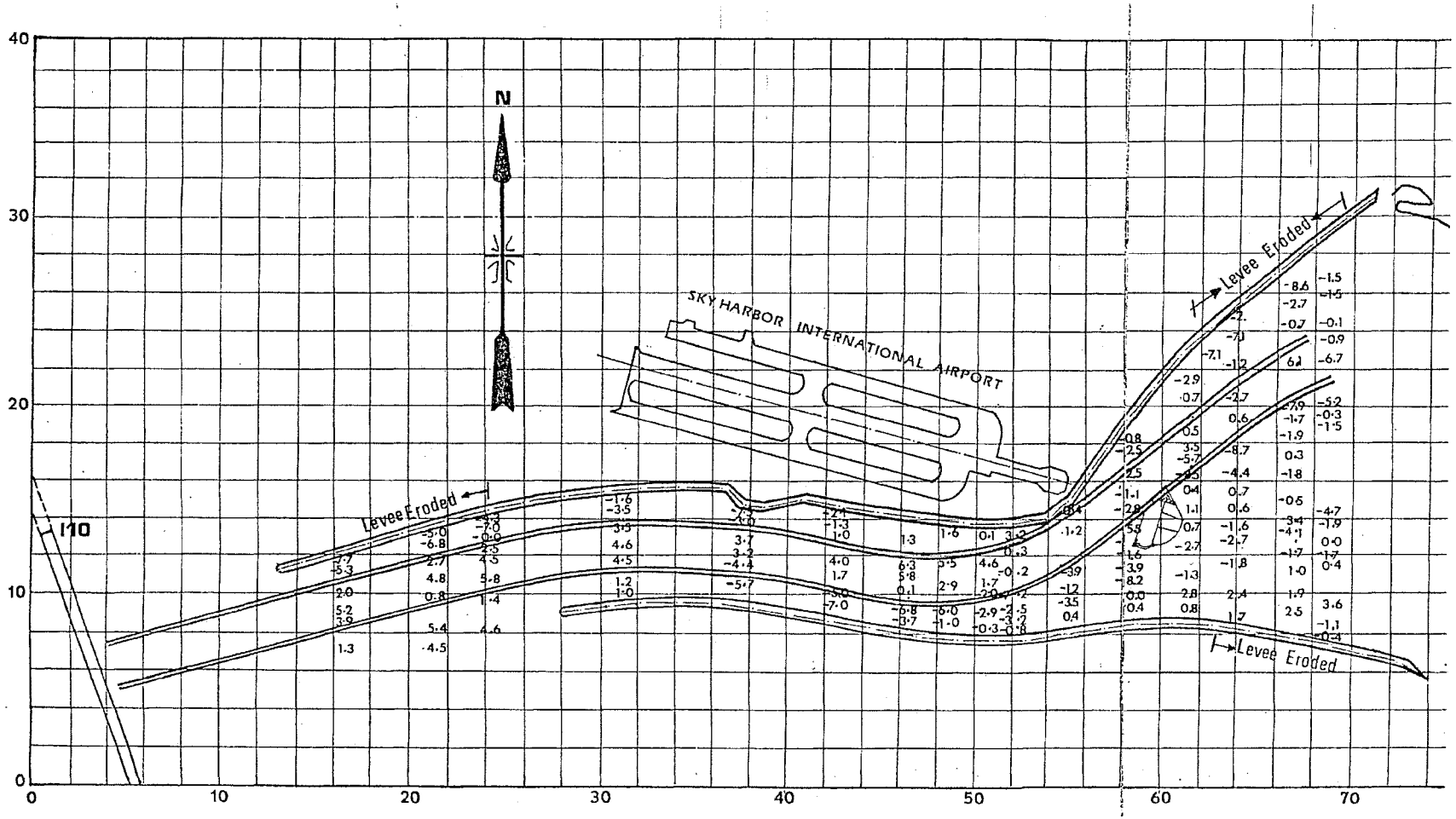

Fig. 24. Bed Elevation Changes from the Initial Values after Routing the Second 92,000 cfs Hydrograph

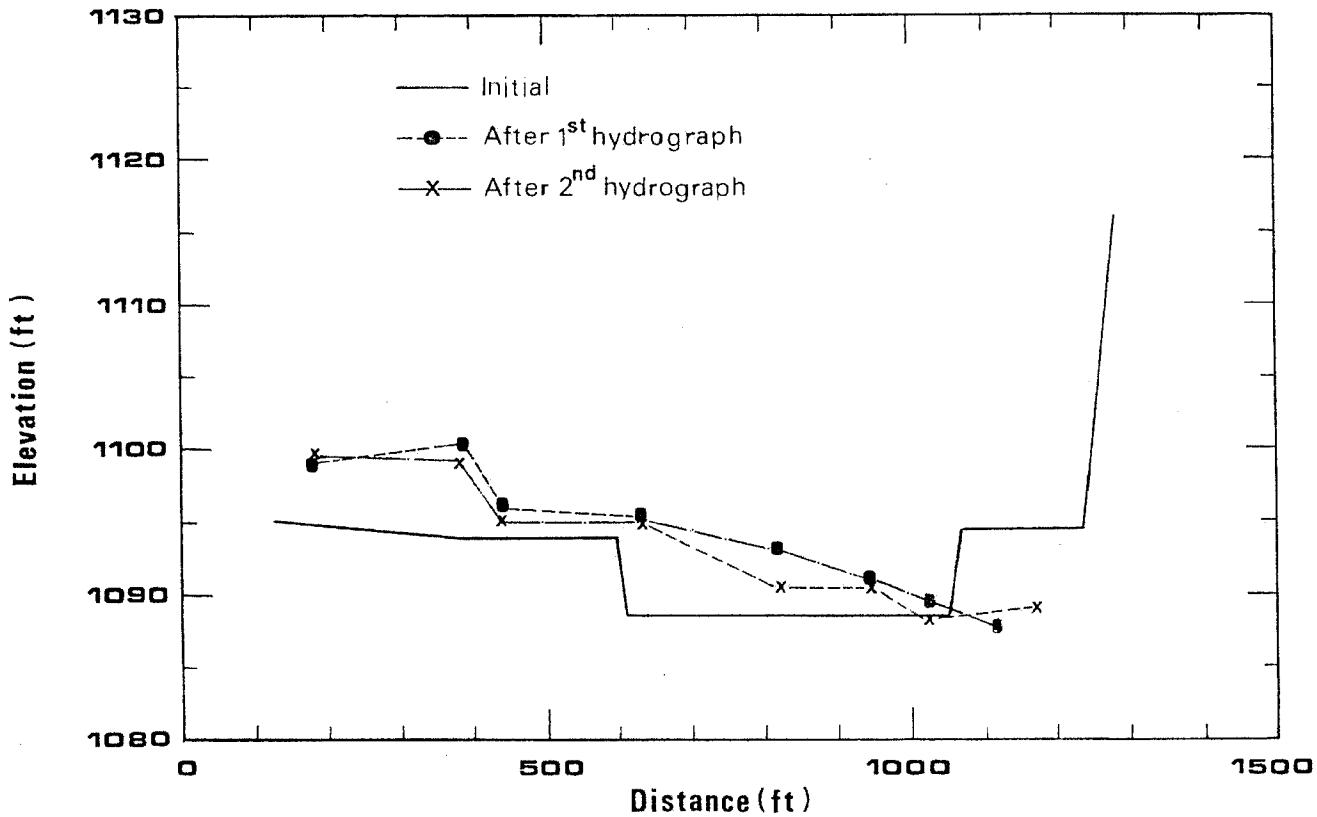

Figure 25. Bed Elevation Changes at Station 21.5 after Routing the 92,000 cfs Hydrographs

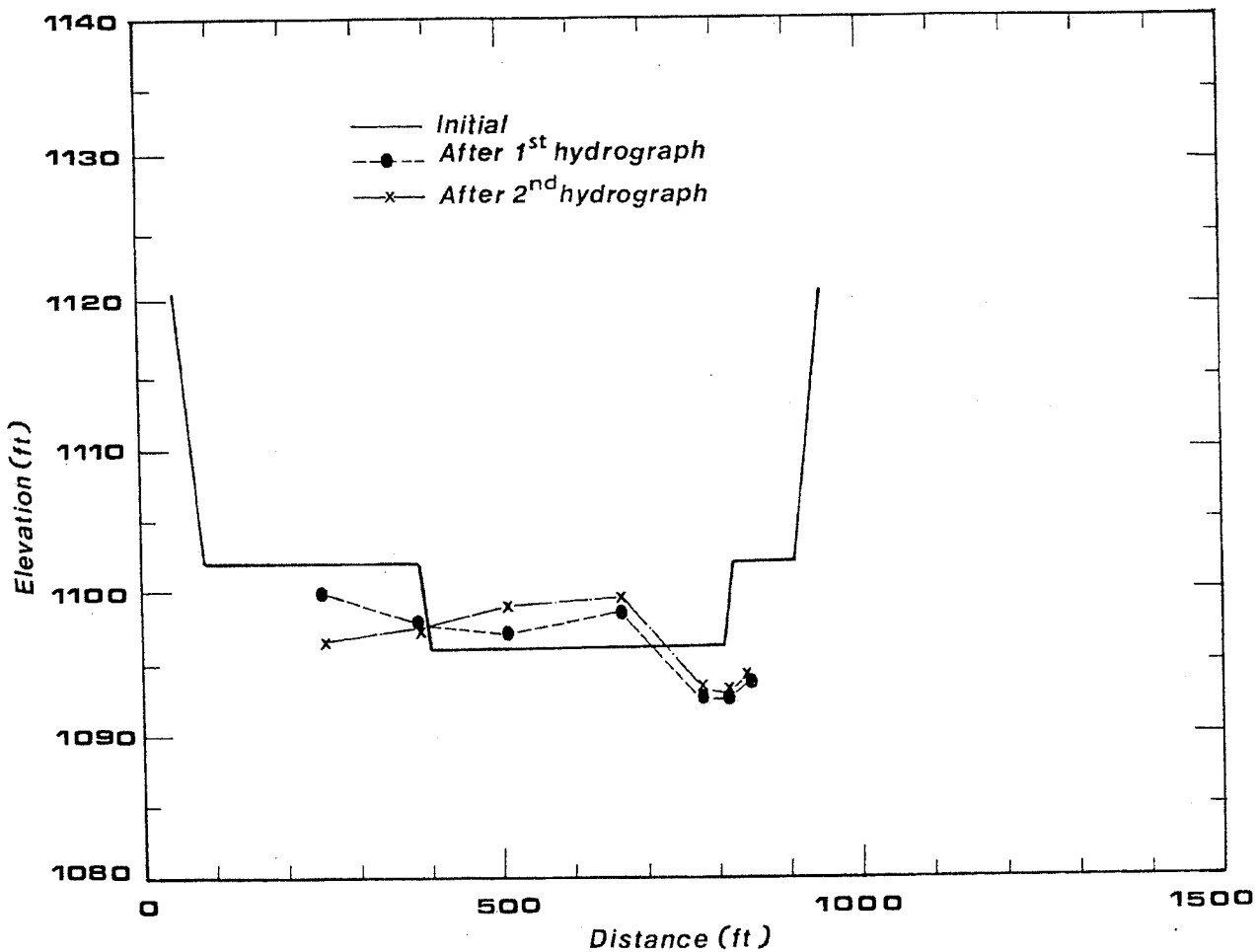

Figure 26. Bed Elevation Changes at Station 37.6 after Routing the 92,000 cfs Hydrographs

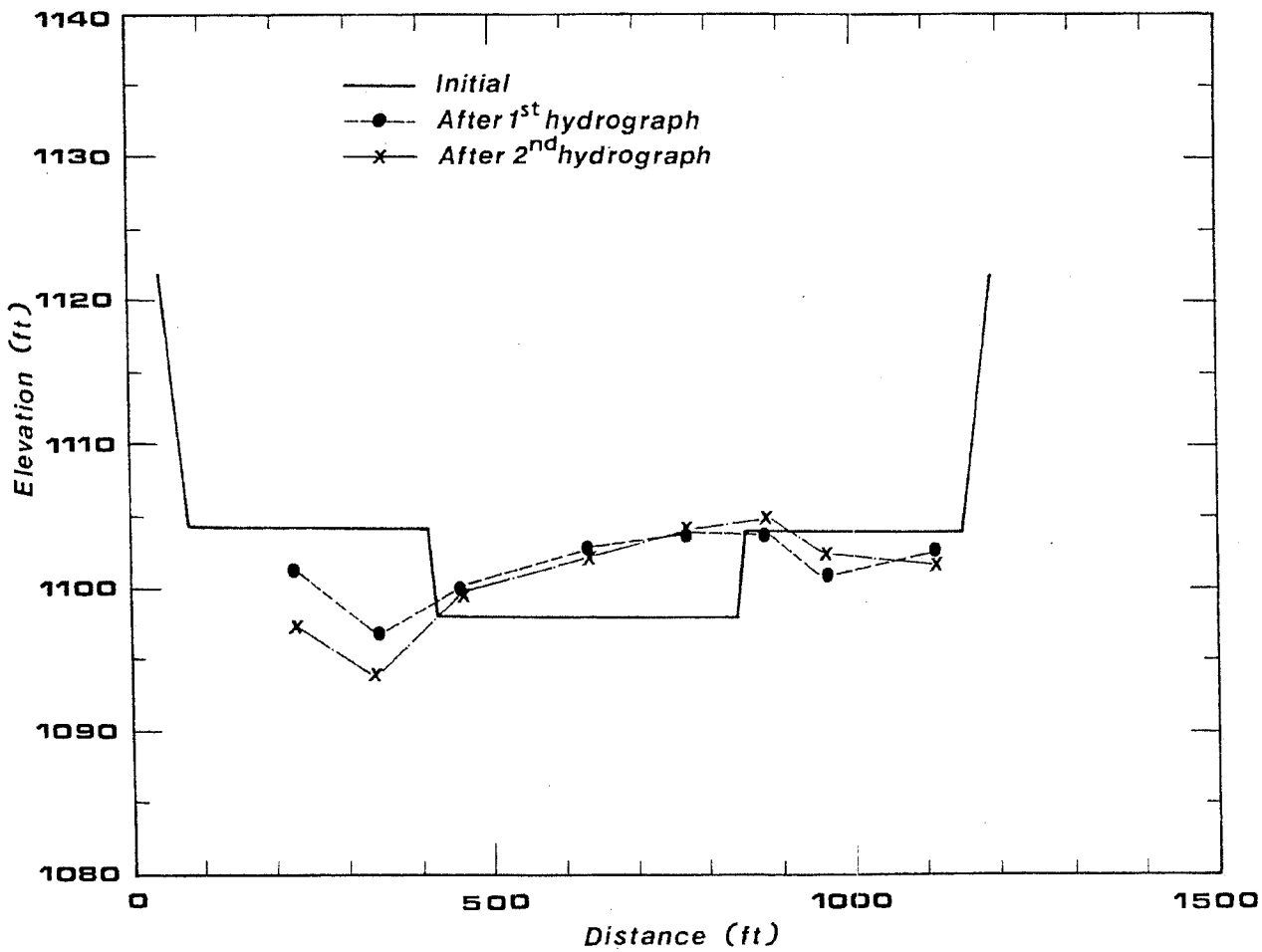

Figure 27. Bed Elevation Changes at Station 42.5 after Routing the 92,000 cfs Hydrographs

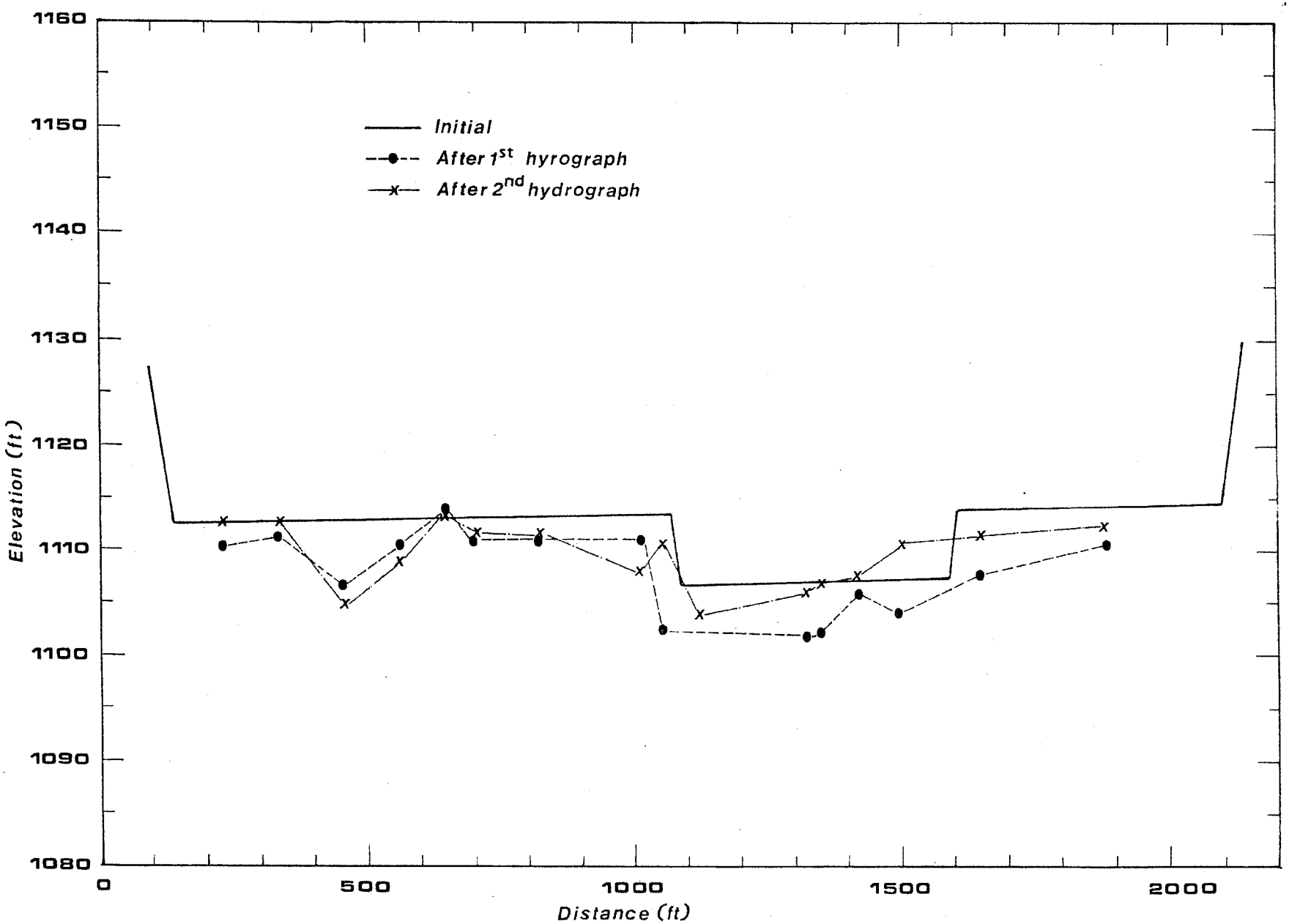

Figure 28. Bed Elevation Changes at Station 58.4 after Routing the 92,000 cfs Hydrographs

routing the 92,000 cfs hydrographs. Some bed elevations in the upper reach of the channelized river were affected by the sediment derived from erosion of the north levee upstream of Station 62 and from erosion of the south levee upstream of Station 63. The low flow channel essentially disappeared after the first 92,000 cfs hydrograph. In general, the low flow channel aggraded and flood plain degraded.

Figures 29 and 30 show the bed contours in the movable-bed model after routing the 210,000 cfs hydrograph. The general erosion and deposition patterns are similar to those after routing the 92,000 cfs hydrographs. The bed elevation changes from the initial contours are given in Figs. 31 and 32 respectively, fcr after the rising limb and after passage of the entire 210,000 cfs hydrograph. Figures 33 through 36 show the changes in cross-sectional shapes at Stations 21.5, 37.6, 42.5 and 58.4. The results of bed elevation changes estimated by SLA for routing a 176,000 cfs hydrograph through a mathematical model are also shown in these figures. It can be seen that the maximum erosion usually occurred during rising limb and it decreased somewhat during falling limb. The results of the CSU physical model and the SLA mathematical model are reasonably close.

Size distribution of bed material on river surface would be altered during transport of sediment and development of erosion and deposition patterns in the channelized river reach. Surface bed material samples were collected at local scour holes, middle bars and point bars in the model, and were analyzed. The size distributions of these samples are plotted in Fig. 37 versus the initial bed material size distribution. It was found that an armoring layer developed at local scour holes and on eroded middle bars, affecting the sediment transport. Bed material with smaller sizes was found to deposit on the point bar near the north

(a) After the rising limb, big scour hole occurred at ILS near the north levee

(b) After the rising limb, point bar occurred between the transition and the radar station near the north levee

(c) Erosion along the lower north levee and deposition in the low flow channel

(d) After the passage of entire hydrograph the depth of scour hole at ILS became shallower, indicating sediment filling during the falling limb

Fig. 29. Photos showing the Bed Surface of the Movable-Bed Model after Routing the 210,000 cfs Hydrograph

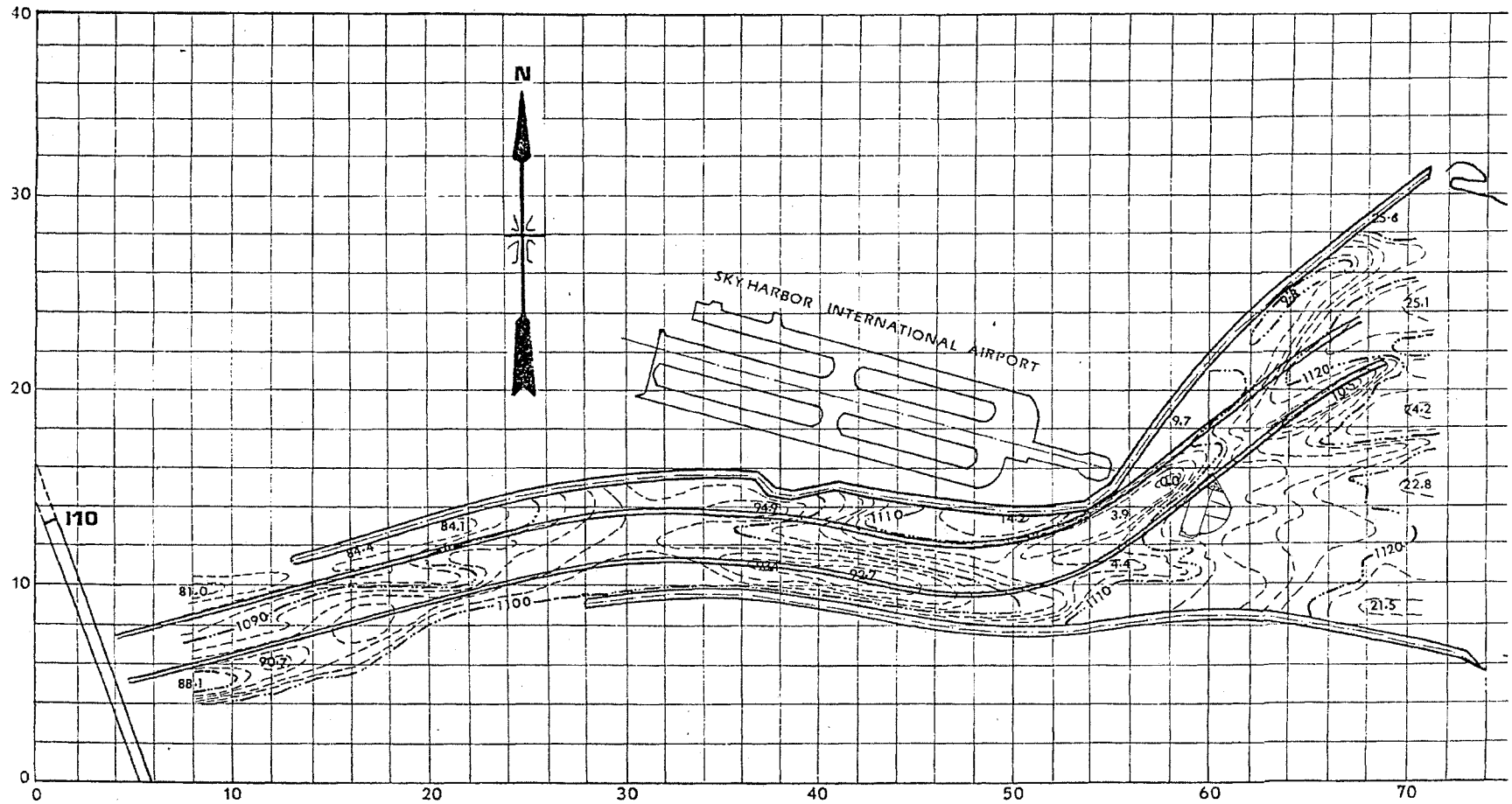

Fig. 30. Bed Contours in the Movable-Bed Model after Routing the 210,000 cfs Hydrograph

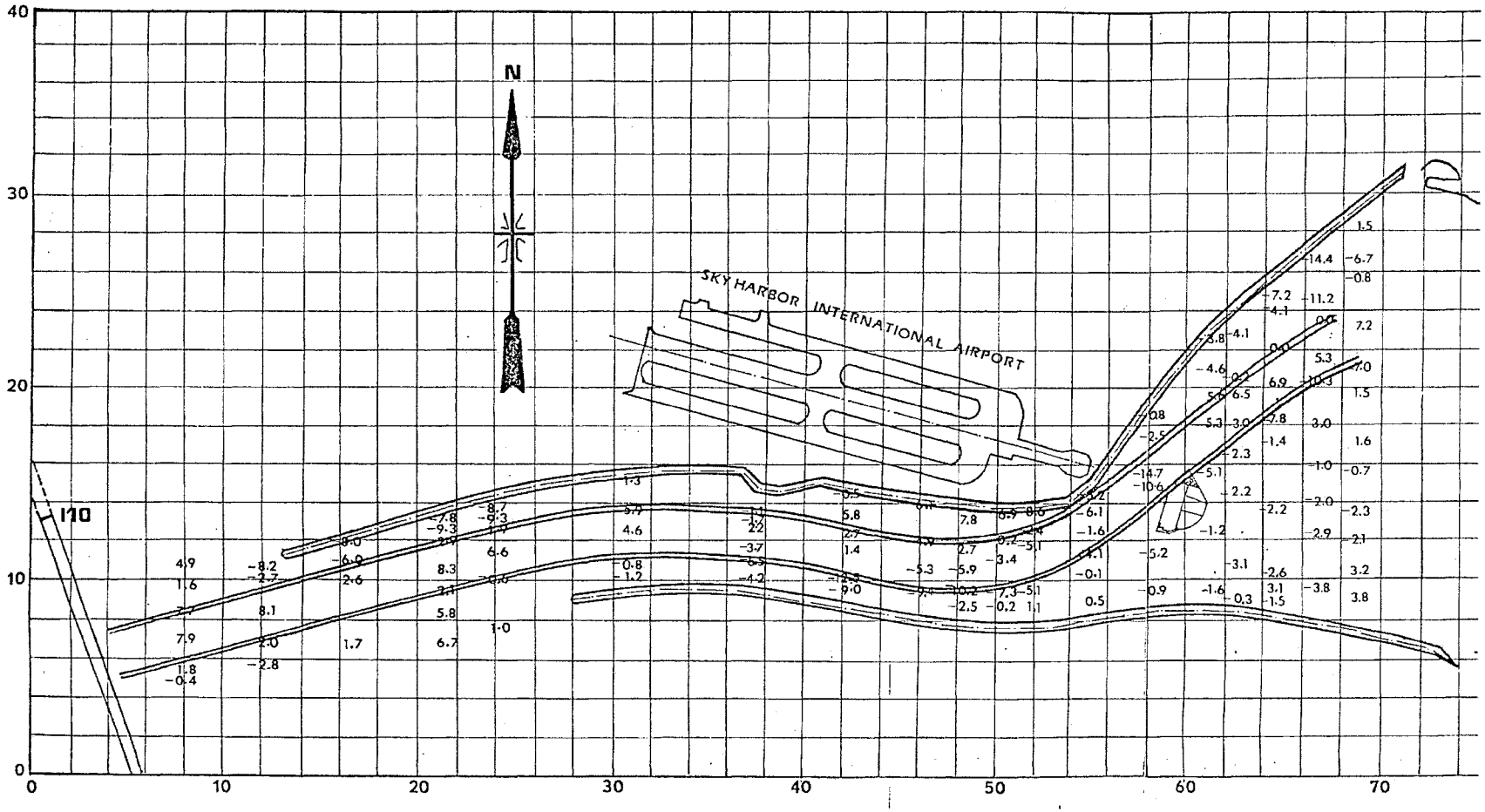

Fig. 31. Bed Elevation Changes from the Initial Contours after the Rising Limb of the 210,000 cfs Hydrograph

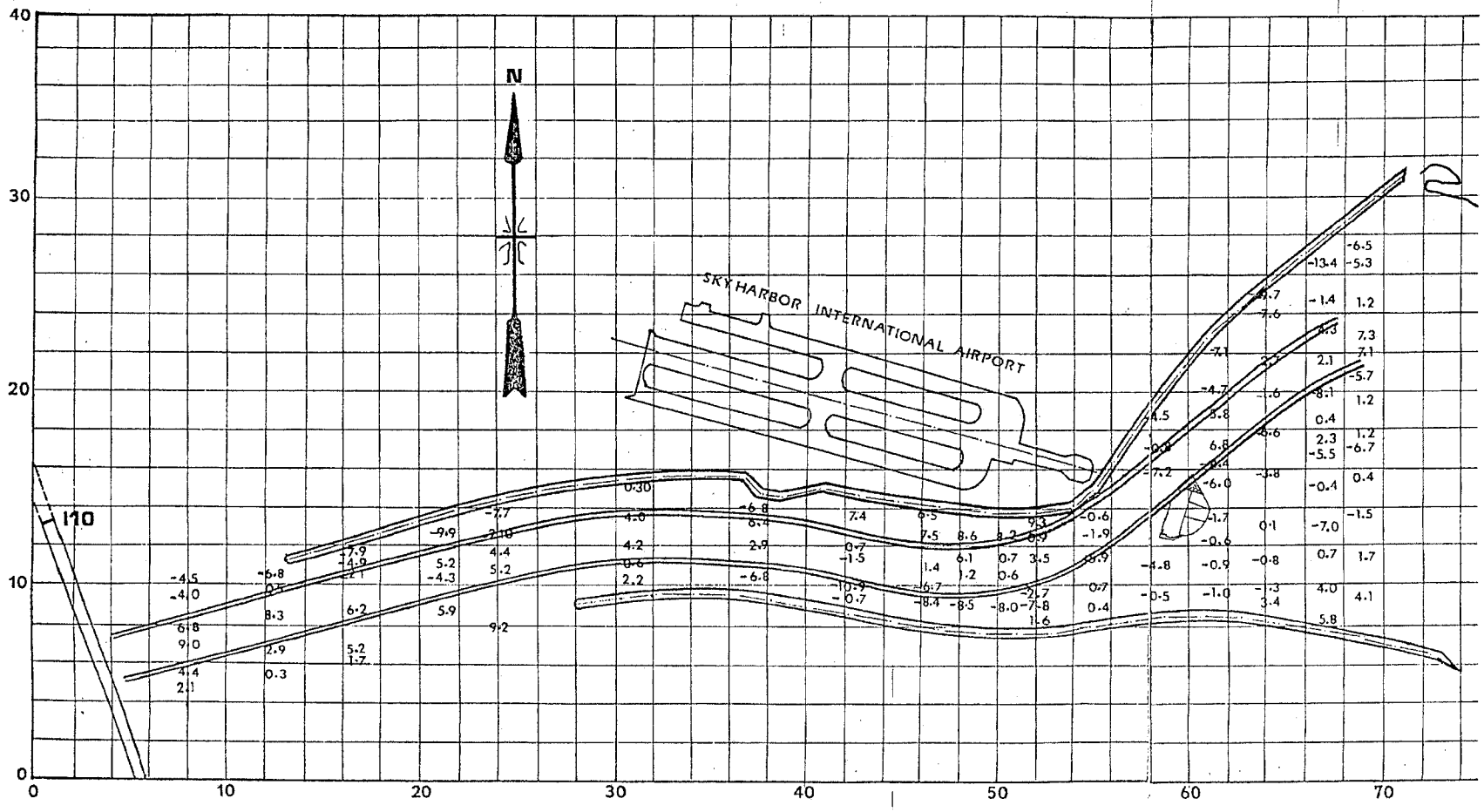

Fig. 32. Bed Elevation Changes from the Initial Contours after Routing the 210,000 cfs Hydrograph

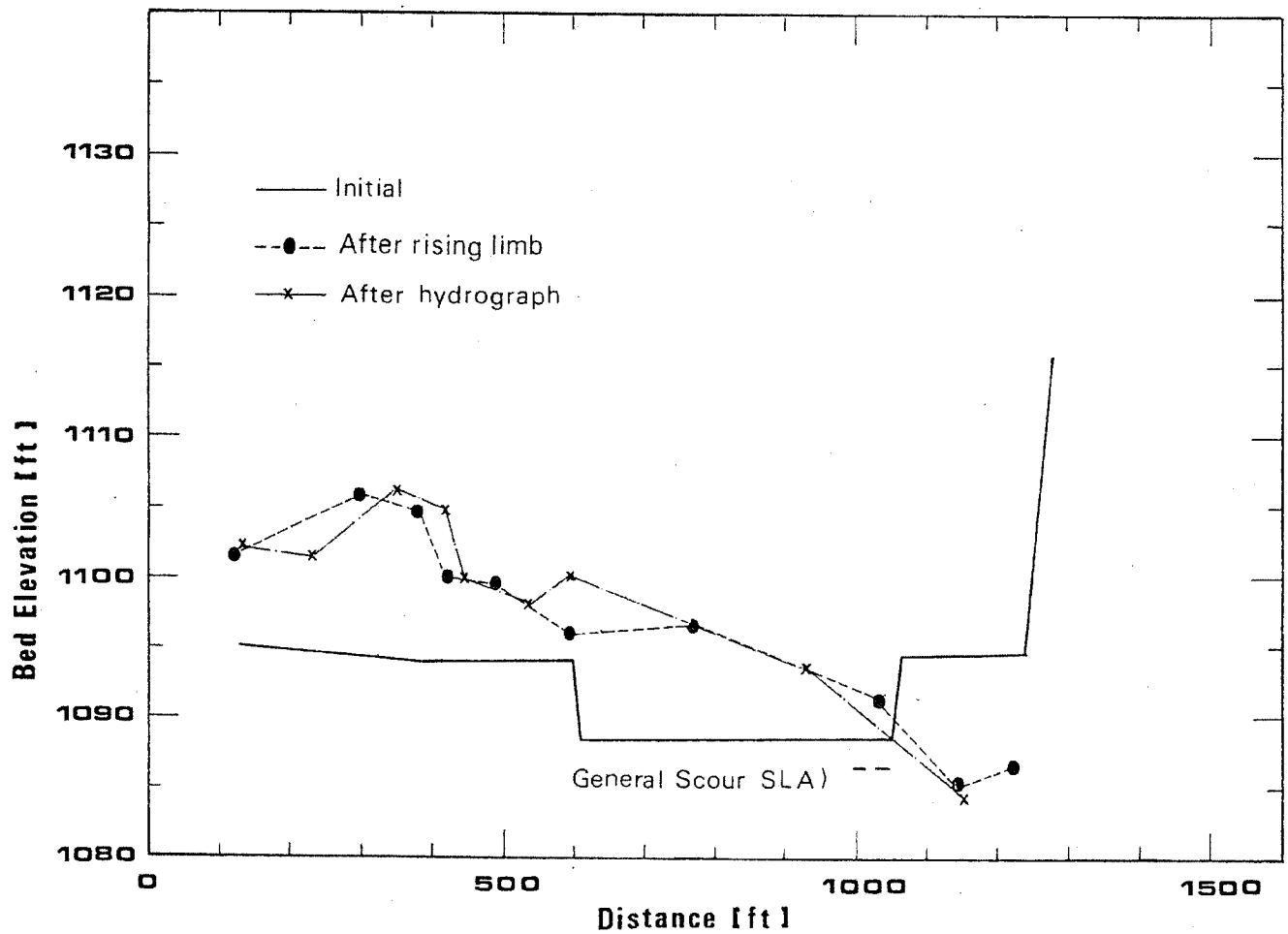

Figure 33. Bed Elevation Changes at Station 21.5 after Routing the 210,000 cfs Hydrograph

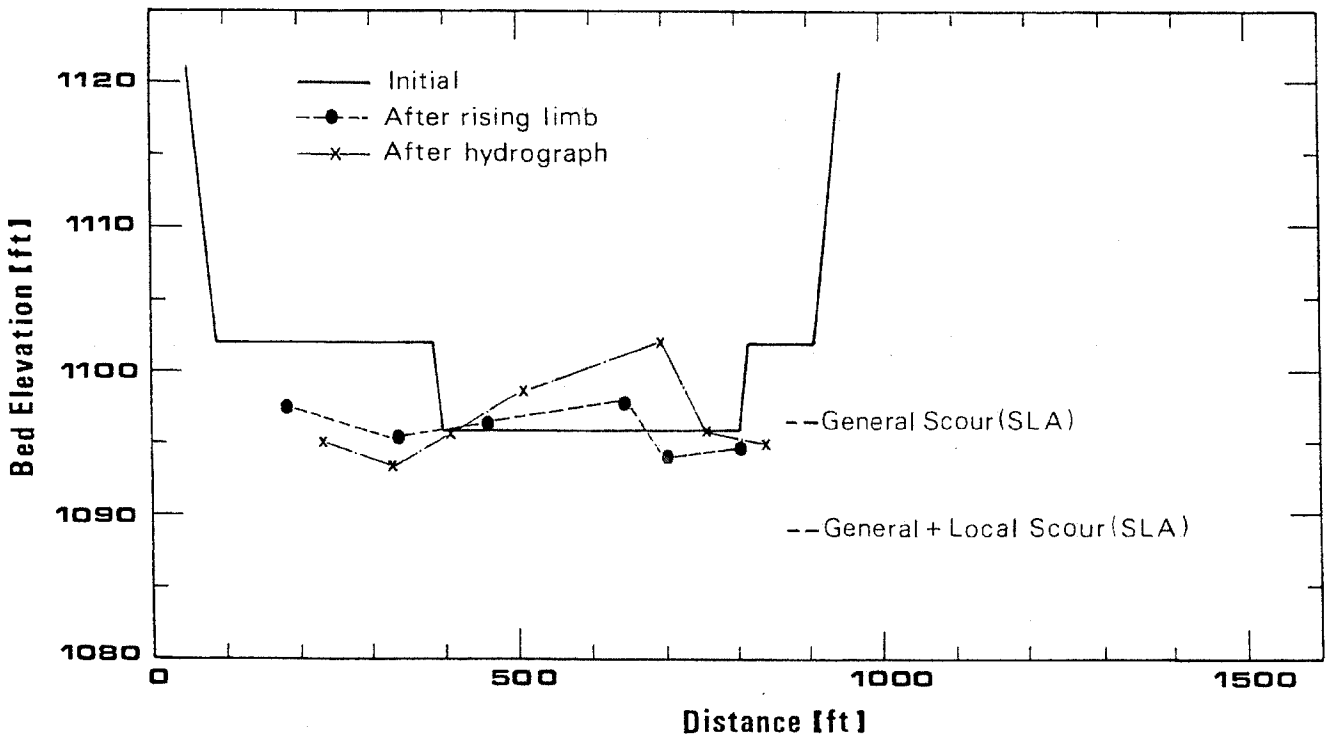

Figure 34. Bed Elevation Changes at Station 37.6 after Routing the 210,000 cfs Hydrograph

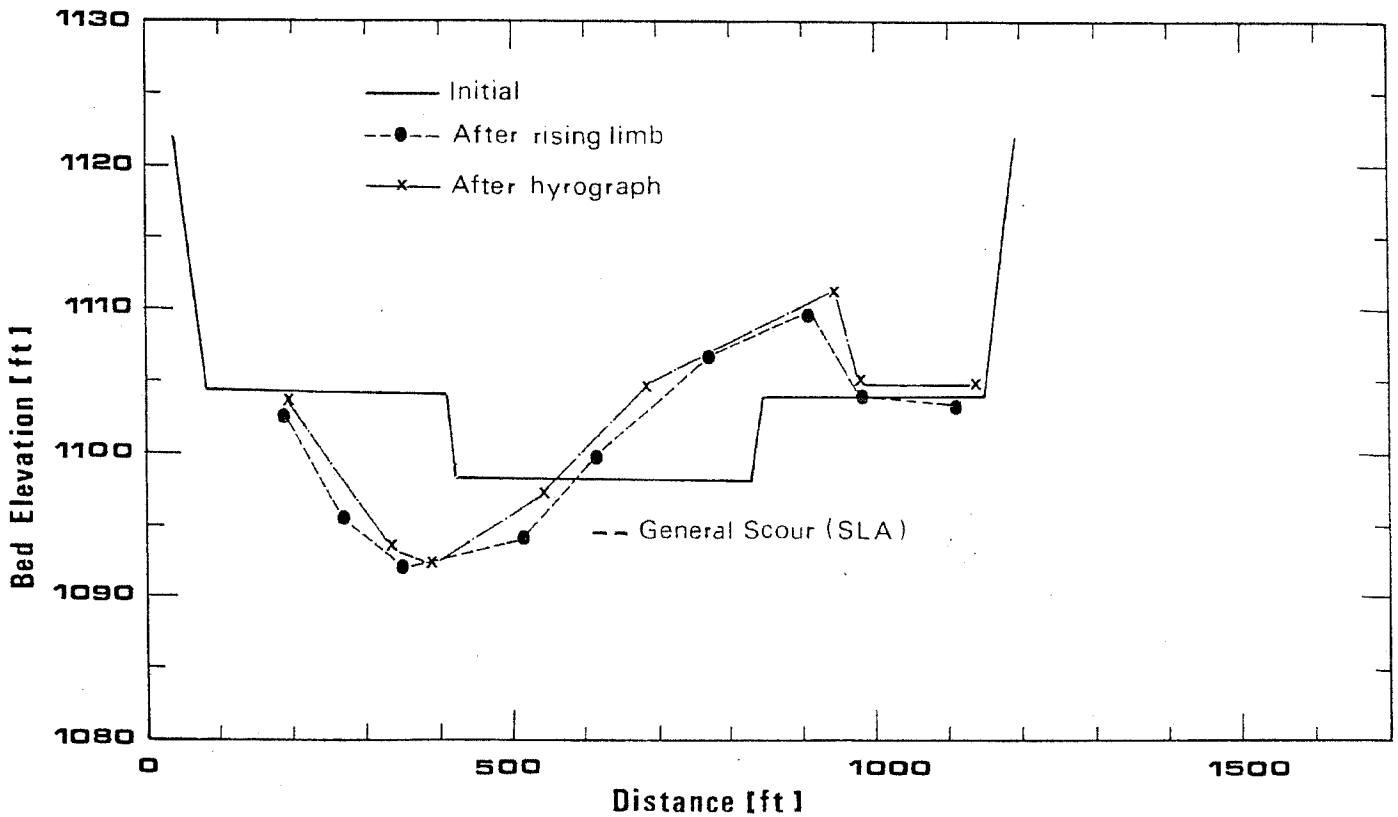

Figure 35. Bed Elevation Changes at Station 42.5 after Routing the 210,000 cfs Hydrograph

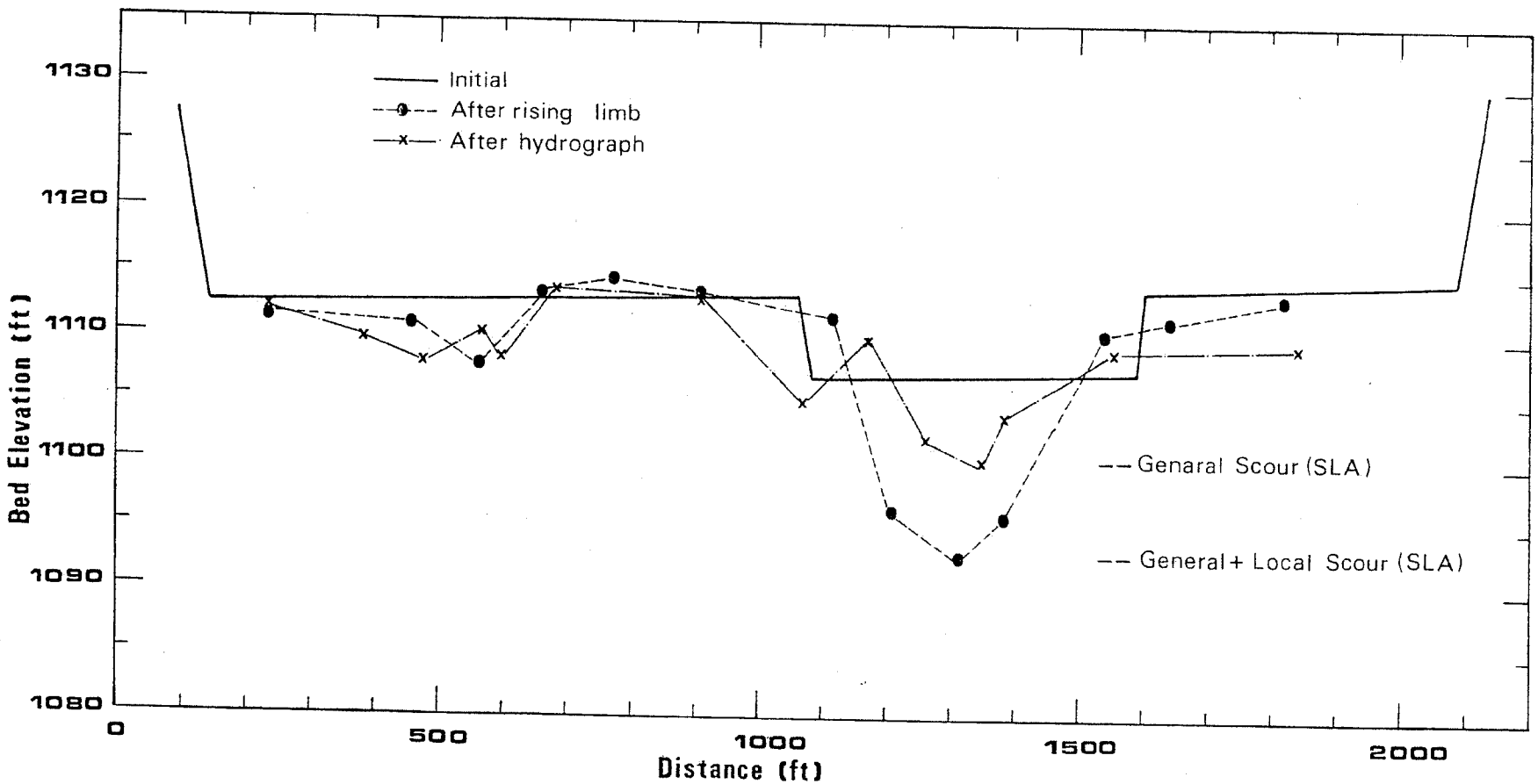

Figure 36. Bed Elevation Changes at Station 58.4 after Routing the 210,000 cfs Hydrograph

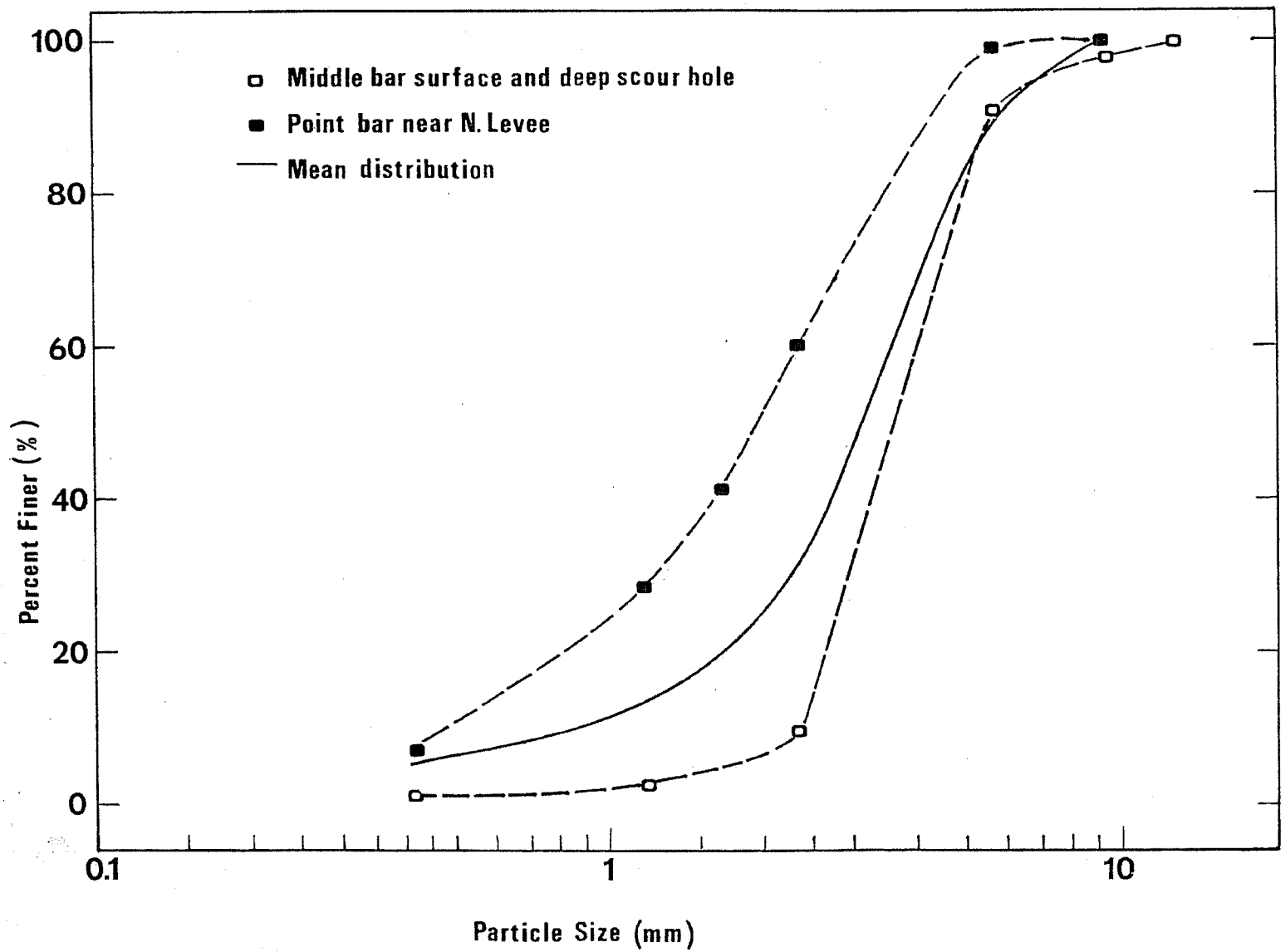

Fig. 37. Change in the Size Distribution of Bed Material on the Model Surface

levee below the transition zone and above the radar station and on some other natural deposition areas such as behind ILS and transmission tower sites.

V.4. Stability of Levees

HNTB proposed to protect the south levee downstream of Station 61 and portions of the north levee as shown in Fig. 13. Protection of these levees should be extended to below the maximum scour depth given in Figs. 23, 24, 31 and 32, to avoid undercutting. Other sections of unstable levees were identified from the model studies. Figures 38 and 39 show photos of these unstable sections. The locations of these sections are given in Fig. 24, identified as eroded levee. It was found that with additional protection for the upstream end of the south levee, the levee system proposed to be protected according to HNTB's plan would last the first 92,000 cfs flood (10-year flood), but it might not last another flood. Without further protection of the unstable levee sections, this levee system may be insufficient to protect the areas against the 210,000 cfs flood (100-year flood).

Evaluation of the levee stability using the movable-boundary model only provides qualitative results. It is not exactly certain under what flood conditions the levee system would not hold.

V.5. Effects of Riverbed Changes on Hydraulics

The riverbed elevation changes affect the flow distributions and stages in rivers. Comparing the rigid-bed model results with the movable-bed model results indicates the following effects:

1) In general, the velocities measured in the rigid-bed model are adequate for design purposes and for evaluating the stabilities of the channelization system. Figures 40 through 43 show the comparison between the velocities measured in the fixed-bed model and in the movable-bed

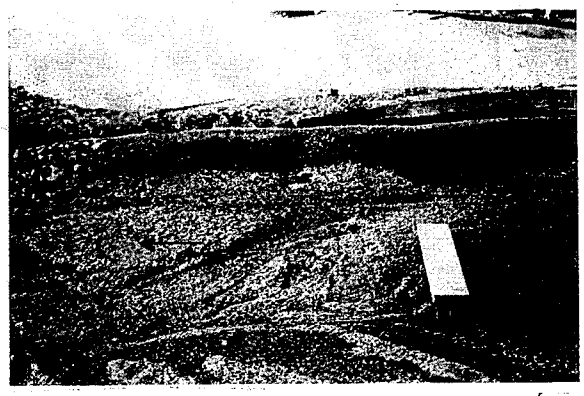

(a) Some erosion of the upper north levee in the transition after the first 92,000 cfs hydrograph

(b) The upper north levee upstream of the protected section was eroded after the second 92,000 cfs hydrograph

(c) Some erosion of lower north levee after the first 92,000 cfs hydrograph

(d) Continuous erosion of the lower north levee after the second 92,000 cfs hydrograph

Fig. 38. Photos showing the Unstable Sections of the North Levee

(a) Flow in chute channel attacked the upstream end of the south end. The levee was then protected

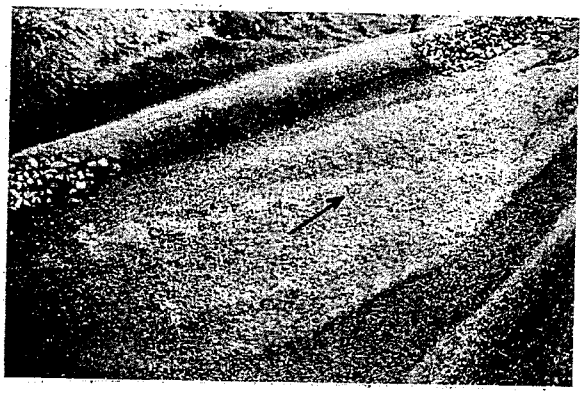

(b) Some erosion of the upper south levee upstream of the ILS after the first 92,000 cfs hydrograph

(c) Further erosion of the upper south levee after the second 92,000 cfs hydrograph

(d) Bed erosion near the south levee downstream of the ILS resulting in sliding of protective riprap

Fig. 39. Photos showing the Unstable Sections of South Levees

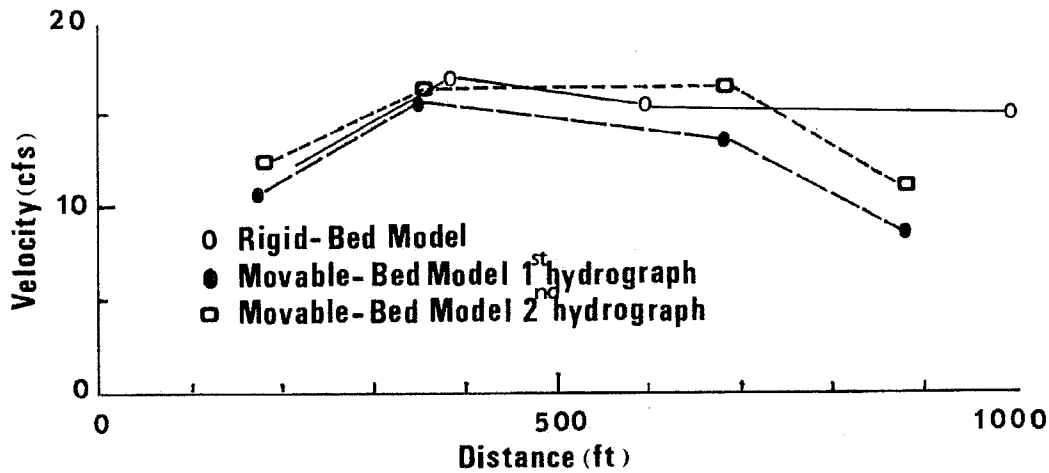

Fig. 40. Comparison between Velocities in the Rigid-Bed Model and in the Movable-Bed Model at Station 38.5 (Q = 92,000 cfs)

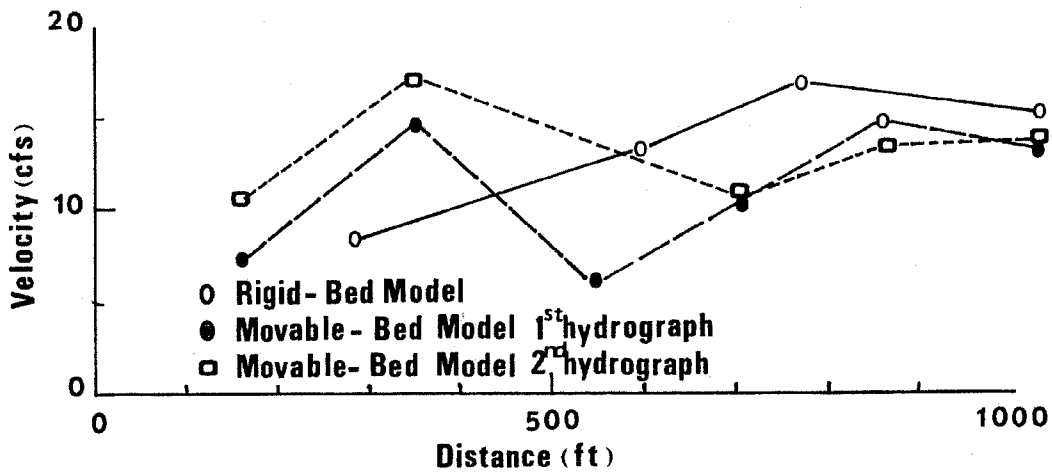

Fig. 41. Comparison between Velocites in Rigid-Bed Model and in the Movable-Bed Model at Station 55 (Q = 92,000 cfs)

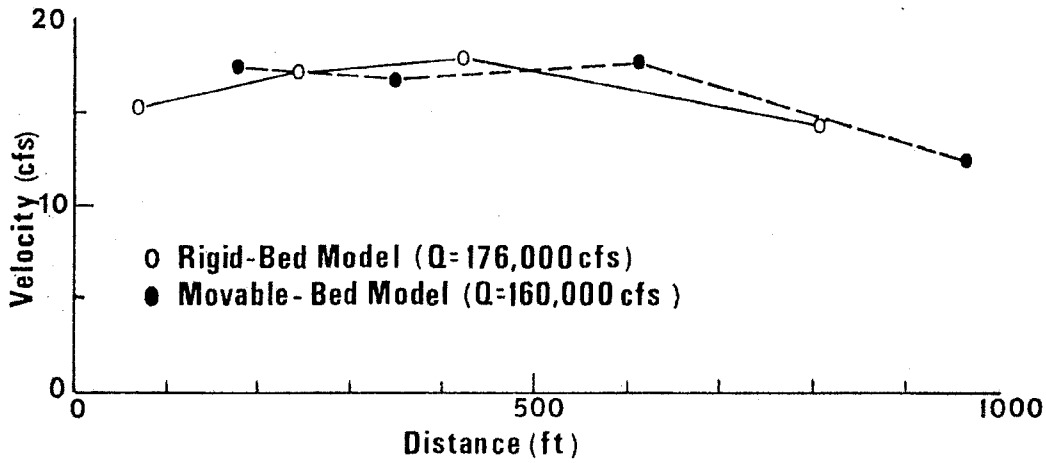

Fig. 42. Comparison between Velocities in the Rigid-Bed Model and in the Movable-Bed Model at Station 38.5 (Q = 160,000 - 176,000 cfs)

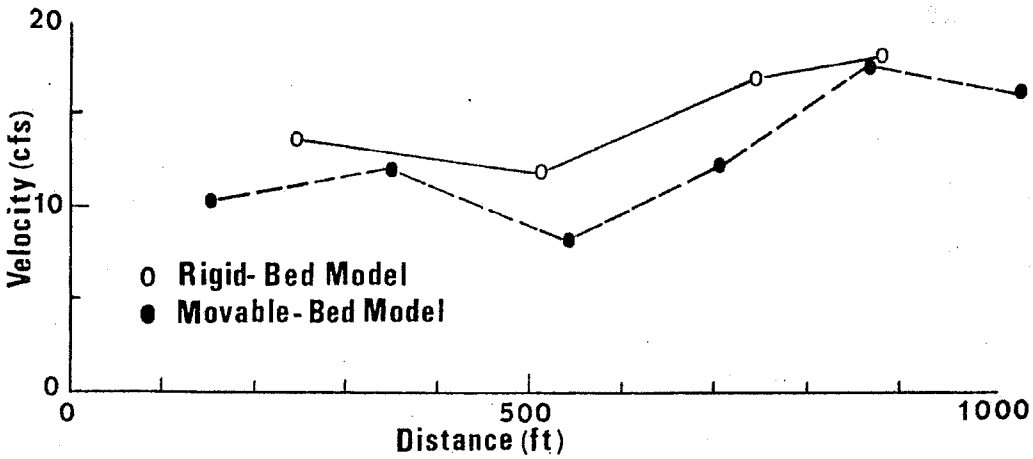

Fig. 43. Comparison between Velocities in the Rigid-Bed Model and in the Movable-Bed Model at Station 55.4 (Q = 210,000 cfs)

model at Stations 38.5 and 55. It is evident that the velocities in these two models are comparable.

2) Bed elevation changes near the ILS also affect the flow distributions passing through the north and south channels separated by the ILS. During routing the first 92,000 cfs hydrograph, the flow discharge passing through the channel south of the ILS was about 31 percent of the total discharge (Q = 73,000 cfs), compared with about 32 percent of total discharge during routing the second 92,000 cfs hydrograph and about 30 percent of total discharge for the rigid-bed model. The reason for this increase in flow distribution is mainly due to the erosion in the south channel caused by the passage of the 92,000 cfs hydrograph. However, during the passage of the 210,000 cfs hydrograph, extensive amounts of material were eroded from the south levee upstream of the ILS. This eroded levee material deposited on the nearby floodplain to divert the flow away from the south channel and thus reduce the flow discharge passing through the channel south of the ILS to about 31 percent of the total discharge (Q = 166,000 cfs), compared with 35 percent of total discharge for the rigid bed model.

3) At Q = 92,000 cfs, the water surface profile in the movable-bed model is essentially the same as in the rigid-bed model. However, at Q = 210,000 cfs, the stage immediately upstream of the radar station increased by about 4 ft, mainly caused by the formation of a point bar during the rising limb of 210,000 cfs hydrograph, near the north levee between Stations 54 and 40, which changed the main flow direction near the radar station and reduced the constriction effect on flow. The distortion in levee slopes might also have some effect on river stage. In addition, sediment wave movement and bed form changes also altered the flow area and resistance to flow to affect the water surface profile in other reaches of river as given in Table 9.

TABLE 9. Changes in Stages between the Movable-Bed Model and the Rigid-Bed Model (Q = 210,000 cfs)

Station	Movable-Bed Model Bed Elevation (ft)		Fixed-Bed Model Bed Elevation (ft)	
	South Levee	North Levee	South Levee	North Levee
23	-	1109.9	-	1108.2
28.5	1112.9	1113.7	1110.0	1111.1
33.2	1113.5	1114.6	1112.0	1111.8
38.5	1116.5	1116.3	1111.1	1112.6
45.4	1119.9	1117.8	1119.2	1117.5
55.0	1123.4	1121.6	1122.2	1120.7

VI. CONCLUDING REMARKS

Based on the model test results, some concluding remarks can be drawn:

1) The velocities measured in the rigid-bed model are adequate for design purposes and for evaluating the stabilities of the channelization system.

2) The low-flow channel would essentially disappear after each major flood (say with a recurrence interval more than 10 years).

3) With additional protection of the upstream end of the south levee, the protected levee system proposed by HNTB should last a 92,000 cfs hydrograph, but it might not last another major flood if the system is not repaired. Furthermore, additional sections of levees, as indicated

in Fig. 24, may need protection if the levee system is to survive a 210,000 cfs hydrograph.

4) The protection of levees should extend to below the maximum scour depth to avoid severe undercutting which could cause failure of levee systems.

5) The riverbed changes significantly affect the flow distributions and stages. The point bar developed along the north levee between Stations 54 and 40 during the rising limb of 210,000 cfs hydrograph would raise the stage immediately upstream of the radar station by about 4 feet at Q = 210,000 cfs. Additional freeboard would be required at this location.

6) Realistic changes in size distributions of bed material on the model surface are observed. An armoring layer has developed at local scour holes and on middle bars. This affects the sediment transport and assists in stabilizing the eroded reaches. Fine bed material deposits on the point bar near the north levee between the transition and the radar station.

7) The levee slopes in the movable-bed model, although being distorted, provide useful information regarding the relative stabilities of levee sections. However, the eroded material from levees affects the erosion and deposition patterns, especially in the upper portion of the model. These effects will be evaluated during the gravel mining model tests where the model will have fixed levee slopes and movable riverbed.